

STATISTICAL STUDY ON THE DECAY PHASE OF SOLAR NEAR-RELATIVISTIC ELECTRON EVENTS

D. LARIO

The Johns Hopkins University, Applied Physics Laboratory, Laurel, MD 20723, USA
Received 2010 February 2; accepted 2010 May 26; published 2010 June 29

ABSTRACT

We study the decay phase of solar near-relativistic (53–315 keV) electron events as observed by the *Advanced Composition Explorer (ACE)* and the *Ulysses* spacecraft during solar cycle 23. By fitting an exponential function ($\exp -t/\tau$) to the time–intensity profile in the late phase of selected solar near-relativistic electron events, we examine the dependence of τ on electron energy, electron intensity spectra, event peak intensity, event fluence, and solar wind velocity, as well as heliocentric radial distance, heliolatitude, and heliolongitude of the spacecraft with respect to the parent solar event. The decay rates are found to be either independent or slightly decrease with the electron energy. No clear dependence is found between τ and the heliolongitude of the parent solar event, with the exception of well-connected events for which low values of τ are more commonly observed than for poorly-connected events. For those events concurrently observed by *ACE* and *Ulysses*, decay rates increase at distances >3 AU. Events with similar decay rates at *ACE* and *Ulysses* were observed mainly when *Ulysses* was at high heliographic latitudes. We discuss the basic physical mechanisms that control the decay phase of the electron events and conclude that both solar wind convection and adiabatic deceleration effects influence the final shape of the decay phase of solar energetic particle events, but not as expressed by the models based on diffusive transport acting on an isotropic particle population.

Key words: acceleration of particles – interplanetary medium – Sun: particle emission

Online-only material: machine-readable tables

1. INTRODUCTION

Since the early years of solar energetic particle (SEP) observations by neutron monitors and balloon-borne neutron detectors, it was soon realized that high-energy (>100 MeV) proton intensities usually show a rapid increase, reach a maximum shortly after the SEP injection from the Sun, and then fall off exponentially at late times (Meyer et al. 1956). In some events, mostly associated with solar flares occurring at the western hemisphere of the Sun, the time–intensity profiles were shown to have a strong peak followed by a period of power-law decay just after the maximum and then an exponential decay at late times (Meyer et al. 1956; Burlaga 1967). For events associated with eastern flares, the time of maximum intensity was less marked, and the entire decay was shown to follow an exponential law (Burlaga 1967).

The first observations of solar near-relativistic ($\gtrsim 40$ keV) electron events (e.g., van Allen & Krimigis 1965; Anderson & Lin 1966) showed time–intensity profiles having “a striking general similarity to corresponding time profiles for $\gtrsim 20$ MeV solar proton events; specifically (1) a sharp onset; (2) an increase to a maximum value in a time of the order of several hours; and (3) a gradual decline over a period of a day or two” (van Allen & Krimigis 1965, p. 5747). The similarity between near-relativistic electron and high-energy ($\gtrsim 20$ MeV) proton time–intensity profiles was also shown by overplotting particle intensities of different species from different experiments (e.g., Figure 6 of Reinhard et al. 1986). Here, we propose to analyze whether the dependence found between the longitude of the parent solar event and the time–intensity profile observed during the decay of high-energy proton intensities (Burlaga 1967) is also observed for near-relativistic (53–315 keV) electron intensities.

McKibben (1972) analyzed solar proton events in the range ~ 10 to ~ 30 MeV observed simultaneously by three spacecraft in the ecliptic plane close to ~ 1 AU but widely separated in

heliolongitude, and showed that the decay phase of the events at at least one of the spacecraft was divisible into two clear phases on the basis of the length of the decay-time constant. Phase 1 was characterized by a relatively short decay-time constant, in the neighborhood of 10–20 hr, whereas the decay constant observed during the Phase 2 was much longer, typically of the order of or greater than 40 hr. For only one of the events analyzed by McKibben (1972) there was no clear evidence for the existence of a fast decay phase at any of the spacecraft. In all of the cases analyzed by McKibben (1972), during Phase 2 the fluxes observed at all three spacecraft were nearly the same, generally within a factor of 2 or 3. This was not true for Phase 1, during which quite pronounced longitudinal gradients could be observed. The change from Phase 1 (with a rapid intensity decay at at least one spacecraft and large spatial intensity gradients between the spacecraft) to Phase 2 (with gradual slow exponential decays and low spatial intensity gradients) occurred several days (typically four) after the onset of the decay of the proton fluxes (McKibben 1972).

The interest in the late phase of the events lies in the observation of heliospheric energetic particle reservoirs, defined as those time intervals when particle intensities measured by widely separated spacecraft (in longitude, latitude, and radial distance) present comparable intensities (within a factor of 2–3) and that evolve similarly in time (McKibben 1972; Roelof et al. 1992; Lario 2010). Heliospheric energetic particle reservoirs are better observed when comparing multi-spacecraft observations of high-energy (>10 MeV) protons and near-relativistic (>30 keV) electrons in the late phase of large SEP events (McKibben et al. 2003; Lario et al. 2003). Particle intensities during these reservoirs usually follow an exponential decay of the form $J \propto \exp(-t/\tau)$ with J being the particle intensity and τ the characteristic decay time of the particle intensity (McKibben 1972; Lario 2010).

Lario (2010) used 175–315 keV electron observation from the *Advanced Composition Explorer (ACE)* and the *Ulysses*

spacecraft to determine when and where near-relativistic electron reservoirs were observed by these two spacecraft. Lario (2010) identified the reservoirs as those periods (1) longer than 12 hr; (2) with electron intensities during the decay phase of SEP events evolving similarly in time at the two spacecraft (the characteristic decay times obtained after fitting an exponential form $J \propto \exp(-t/\tau)$ over the selected time interval at *Ulysses* τ_{Uly} and *ACE* τ_{ACE} had to differ by less than 30%); and (3) with similar intensities at both spacecraft (the average of the logarithms of the intensities over the selected time interval at the two spacecraft had to differ by less than 3%). Those time intervals were selected regardless of the occurrence of one or more SEP injections at the Sun or the observation of one or more SEP events at 1 AU. Near-relativistic electron reservoirs were observed during intense active periods after either a sequence of SEP events at 1 AU or after the occurrence of a large single SEP event (see Figure 1 in Lario 2010). Whereas the occurrence of a single SEP injection favors the observation of near-relativistic reservoirs (such as in 2000 November and 2001 November when *Ulysses* was at high ($>70^\circ$) heliographic latitudes), multiple SEP injections make the observation of the reservoirs more difficult. The average delay between the main peak intensity observed at 1 AU and the onset of the time interval selected as reservoir was of ~ 8 days with a clear difference if the reservoir was observed after a sequence of events at 1 AU (averaged delay of up to ~ 13 days after the main event observed at 1 AU) or if the reservoir resulted from a single large SEP event (average delay of ~ 3 days between the peak intensity at 1 AU and the onset of the reservoir). See details in Lario (2010).

In this paper we propose to study the decay of solar near-relativistic (53–315 keV) electron intensities on an event-by-event basis. Instead of using multi-spacecraft observations to select intervals in the decay phase of SEP events constituting a heliospheric energetic particle reservoir, here we choose single SEP events regardless of whether a reservoir was observed during their decay. In this study, we neglect the fast decay phase observed just after the peak of the event (if observed at all) and study only the late decay phase of the events where presumably the same mechanisms leading to the formation of heliospheric energetic particle reservoirs operate. We use 53–315 keV electron intensities observed (1) near the ecliptic plane at 1 AU from the Sun by the *ACE* spacecraft, and (2) at high and low heliographic latitudes (Λ) and heliocentric radial distances (R) ranging from 1.34 to 5.41 AU by the *Ulysses* spacecraft. Electron intensities used in this paper were measured by the Deflected Electron (DE) telescopes of the Electron Proton and Alpha Monitor (EPAM) on board *ACE* (Gold et al. 1998) and the Heliosphere Instrument for Spectra, Composition, and Anisotropy at Low Energies (HI-SCALE) on board *Ulysses* (Lanzerotti et al. 1992). The similarity between both instruments (EPAM was the spare instrument of HI-SCALE) allows an easy and direct comparison between the results obtained from the two spacecraft.

Statistical studies of the decay phase of SEP events have been mostly focused on proton observations (e.g., Daibog et al. 2003; Kecskeméty et al. 2009, and references therein). Daibog et al. (2003), on a sample of ~ 700 events collected during almost three solar cycles, concluded that in nearly 90% of the cases for 1–5 MeV proton fluxes, an exponential decay gives the best approximation to the time–intensity profiles. At higher energies (above ~ 20 MeV) the fraction of exponential declines with respect to those best described by a power law was smaller. In the statistical study of Daibog et al. (2003),

only those portions of the declines that could reasonably be described by an exponential law were selected. However, no indication of when these exponential decays occurred within the time–intensity profile or whether there were more than one time interval selected within the same event was provided. In this paper we study near-relativistic electron decays that allow a good representation by an exponential law occurring usually after the first rapid decay (if observed). By neglecting the first fast decay after the peak intensity (if any) and selecting only the phase of the decay that follows a slow exponential decay, we neglect whether the whole decay of the event might be better represented by a power law. As pointed out by several authors (e.g., Burlaga 1967), in the case of protons, this exponential phase of the decay usually occurs late in the event for those generated in association with western flares. Here, we analyze whether this dependence between the exponential phase of the decay and the longitude of the parent event is also observed in the case of near-relativistic electrons.

Recently, Daibog et al. (2009) compared the decay rate of 7.8–25 MeV proton and 250–700 keV electron fluxes simultaneously measured by *SOHO*/COSTEP and concluded that nearly half of the clearly shaped electron and proton intensity decays have similar character (exponential or power law), suggesting that at least in part of the events, electrons can be subject to the same propagation mechanisms as protons. Similarly, the resemblance between MeV electron and >30 MeV proton intensity profiles observed by *Ulysses* during large SEP events led McKibben et al. (2003, p. 1225) to state that “the relatively clean profiles observed for electrons with energies of 2 or 3 MeV suggest that velocity may be more important than energy or rigidity in determining the appearance of the time–intensity profiles.”

The most recent study on the decay rate of SEP events was performed by Kecskeméty et al. (2009). These authors studied the decay phase of 0.5–48 MeV proton events observed by the Interplanetary Monitor Platform (*IMP-8*) near the ecliptic at ~ 1 AU from the Sun between 1973 and 2001. Following Daibog et al. (2003), Kecskeméty et al. (2009) selected time intervals during the decay of the events that could “reasonably” be approximated by an exponential. Within the declines of the particle intensities, Kecskeméty et al. (2009) distinguished various time intervals (no shorter than 12 hr) that could be fitted by exponential decays of the same or different decay rate within the same event. Sometimes these exponential decays could last from the maximum of the event to the background intensity, other times they were seen during a part of an event only, were followed by large fluctuations, and then they could become exponential again with the same or different decay rate. Therefore, the database of the statistical study performed by Kecskeméty et al. (2009) are decay rates observed within the decay of the SEP events and not the SEP events themselves. Apart from the different particle species (protons versus electrons) and the selection criteria used in the present work (see Section 3), the statistical analysis of Kecskeméty et al. (2009) or Daibog et al. (2003) and the one presented here differ in the fact that here we use only one decay per event and, when the two decay phases are distinguishable, we choose to neglect the first rapid decay (if observed). Throughout the different sections of the paper, the results found in the present work will be compared with the results of Kecskeméty et al. (2009).

The structure of the paper is as follows. In Section 2, we discuss the main factors that determine the decay phase of the SEP events and which ones can be checked from the statistical analysis of the decay rates presented here. In Section 3, we

describe the criteria used to select the events to study their decay phases and the approach used to determine the decay rate of the events. In Section 4 we present the statistical analysis of the decay rates observed in the energy channels 53–103 keV and 175–315 keV of the EPAM instrument on board *ACE*. In Section 5, we discuss possible dependences between the decay rates observed by *ACE* and the heliolongitude of the solar phenomena associated with the origin of the electron event. In Section 6, we follow the same structure as Section 4 to discuss the results obtained from the *Ulysses*/HI-SCALE/DE observations. In Section 7, we study the possible correlations between the decay rates and the parameters of the solar wind and particle intensities to determine the role that solar wind convection and adiabatic deceleration effects play in shaping the decay phase of the SEP events. In Section 8, we study the decay phase of those events commonly observed by *ACE* and *Ulysses* to determine the radial and latitudinal dependence of the decay rates. Finally, in Section 9 we summarize the main results of the present study.

2. FACTORS DETERMINING THE DECAY PHASE OF SEP EVENTS

During the decay phase of an SEP event the observer does not stay in the same magnetic flux tube (understood as the channel where SEPs propagate primarily along it), rather the spacecraft samples time histories from different flux tubes as they are convected over the observer by the solar wind. Therefore, the observed time–intensity profiles are always a mixture of different magnetic flux tubes with their own characteristics. The factors that determine the properties of the decay phase of an SEP event are the following.

1. The energetic particle transport conditions along and across the different magnetic flux tubes that sweep over the spacecraft through the decay phase of the event.
2. The spatial gradients of the energetic particle intensities as the spacecraft moves from flux tube to flux tube. If there is an effective transport of particles across the field lines or an efficient redistribution of particles among the flux tubes at some location in the heliosphere, such spatial gradients should smooth with time.
3. The speed at which the populated flux tubes move over the observer.
4. The global state of the interplanetary plasma and magnetic field moving over the spacecraft during the decay of the event. In particular, the existence of magnetic field regions in the interplanetary medium (such as interplanetary shocks driven by the interplanetary counterpart of coronal mass ejections (ICMEs) or compressed magnetic field structures formed by solar wind stream interaction regions (SIRs)) capable of producing the confinement of energetic particles traveling between the strong magnetic field near the Sun and such field regions. As this volume expands the whole population contained in it decays with time.
5. The evolution of the particle sources and how the observer establishes magnetic connection with them. That includes how and when the sources filled the different flux tubes that sweep over the spacecraft (i.e., prompt injection of SEPs versus continuous injection of SEPs by a traveling shock).

The first studies of the time dependence of the intensity of SEP events suggested that diffusion played an essential role in the transport of SEPs (e.g., Krimigis 1965 and references therein). Transport models based on the diffusion of energetic particles,

first without and later with convection and adiabatic deceleration effects, were proposed to explain the time–intensity profiles of SEP events (Meyer et al. 1956; Krimigis 1965; Burlaga 1967; Englade 1971; Forman 1971). The early solutions of Meyer et al. (1956) and Burlaga (1967) did not consider convection and obtained power-law decays. In order to reproduce exponential decays, they required a free escape boundary at a finite distance from the Sun. Numerical and analytical solutions by Englade (1971), Forman (1971), and Lupton & Stone (1973) added convection and deceleration to the interplanetary propagation model of Burlaga (1967), including also large perpendicular diffusion coefficients and a free escape boundary at some distance <10 AU. The free escape boundary was located at such a large distance from the Sun that it had little effect on the propagation of SEPs at least in the early phase of the SEP event. As suggested by Meyer et al. (1956), the outer boundary, apart from allowing escape of particles through a barrier formed by irregular magnetic fields, was also capable of scattering particles back to the observer and thus determine the observed rate of declining intensity. All these transport models assumed isotropic particle distributions and neglected the effect of focusing along the magnetic field. This assumption is not well supported by SEP observations especially in the inner heliosphere where magnetic field magnitude decreases rapidly with increasing distance from the Sun making the focusing effect (and hence particle anisotropies) an important factor in the transport of SEPs (Roelof 1969). Although particle populations are usually near-isotropic during the decay phase of the SEP events, particles observed during these decay phases may propagate to distances close to the Sun and be mirrored by the increasing magnetic field there. Therefore, unless there is a strong diffusion of particles by enhanced scattering processes near the spacecraft location, focusing effects must be included when dealing with particle transport during the decay phase of the events.

Transport models including the effects of streaming along field lines, pitch-angle scattering (conveniently parameterized by a diffusion coefficient), focusing, solar wind, and adiabatic deceleration effects (e.g., Ruffolo 1995) show that the decay of the late phase of the time–intensity profiles (produced by an SEP injection close to the Sun) is approximated by an exponential decay that depends on (1) the assumed particle mean free path, (2) the parameterization of the adiabatic deceleration effect that, in general, is a function of the energy spectra of the particle intensity, (3) the solar wind speed that determines the solar wind convection effect, and (4) the duration of the particle injection. Ruffolo (1995) showed how the decay rate (approximated by an exponential decay time constant) varies in terms of each one of these factors (see his Figure 8).

Among the different factors that determine the decay phase of the SEP events, it is readily easy to observationally check the role that solar wind convection and adiabatic deceleration effects have in shaping the decay of the SEP events. A correlation between solar wind speed V_{sw} and decay rate should be expected if solar wind convection determines the decay phase of SEP events (Kecskeméty et al. 2009). As magnetic flux tubes move with the solar wind speed over the observer, one should expect faster decays for faster solar wind. The effect of adiabatic deceleration in the decay phase of SEP events should translate into a faster decrease of particle intensities in a given energy range the faster the particle intensities decrease with energy (i.e., the softer the energy spectrum the faster the decrease of the particle intensities with time).

The possible effects of particle scattering and cross-field diffusion are difficult to determine from the decay phase of the events since theoretical expressions given for the decay rates (in the case of diffusive transport models; e.g., Lupton & Stone 1973; Owens 1979) depend on the diffusion coefficients that may vary from event to event and along the field lines where SEPs propagate. A detailed modeling of the SEP transport to fit the observed time–intensity profiles (together with particle anisotropies) is required in order to estimate the SEP transport conditions (such as the scattering mean free path) for each event (e.g., Agueda et al. 2008 and references therein). Because of the large number of events, such approach is not practical for statistical analyses such as the one presented in this work.

In order to determine the role that spatial intensity gradients have in each event, it would be necessary to have observations from multiple inter-calibrated distant spacecraft and thus separate in each event the spatial from the temporal variations (e.g., Reinhard et al. 1986). Multispacecraft observations suitable to do this study are not usually available. Finally, the existence of magnetic field structures beyond the observer location able to reflect energetic particles back to the observer (e.g., Anderson et al. 1995; Sarris & Malandraki 2003) can only be partially inferred from single-point observations. Uncertainties about (1) the magnetic connection established between these distant structures and the spacecraft, (2) the capability of these structures to reflect energetic particles back to the observer, and (3) the evolution of these structures as they move away from the observer are inherent in the study of the decay phase of the events based only on single-spacecraft observations.

Therefore, among the factors that determine the decay rate of the SEP events we will check the influence of solar wind convection and adiabatic deceleration effects, and explore the possibility that spatial gradients shape the decay phase of the SEP events.

3. EVENT SELECTION

The database used for our statistical analysis consists of near-relativistic electron events measured by the DE system of the EPAM and HI-SCALE instruments on board *ACE* and *Ulysses*, respectively. We have scanned hourly averaged near-relativistic electron increases from 1997 November to 2007 December. This time interval comprises almost the whole active period of solar cycle 23 (Lario 2007). We have considered all events in which (1) the 175–315 keV electron peak intensity is above 5×10^1 electrons $(\text{cm}^2 \text{ s sr MeV})^{-1}$, (2) the 175–315 keV electron peak intensity is at least a factor of 1.2 above the intensity measured just before the onset of the event (hereafter the pre-event intensity), (3) the time–intensity profile in the decay phase of the event follows an exponential time dependence; i.e., a least-squares fit to the profile of the particle intensity (after subtraction of the pre-event intensity) with a function $\ln(J) = \ln(J_0) - (t - t_0)/\tau$ should provide a good approximation to the observations with a regression coefficient always above 0.9, and (4) the time interval over which the decay phase follows a $J \propto e^{-t/\tau}$ dependence is longer than 12 hr.

Figure 1 shows two examples of the events analyzed. The thin black traces show the hourly averaged 175–315 keV intensities as measured by *ACE/EPAM/DE*, whereas the thick gray traces show the intensities after subtraction of the pre-event intensity (indicated by the thick black solid horizontal line prior to the onset of the event). Note that the gray traces have been scaled down by a factor of 10^{-1} . The two thin vertical lines indicate the time interval selected for the analysis of the decay phase.

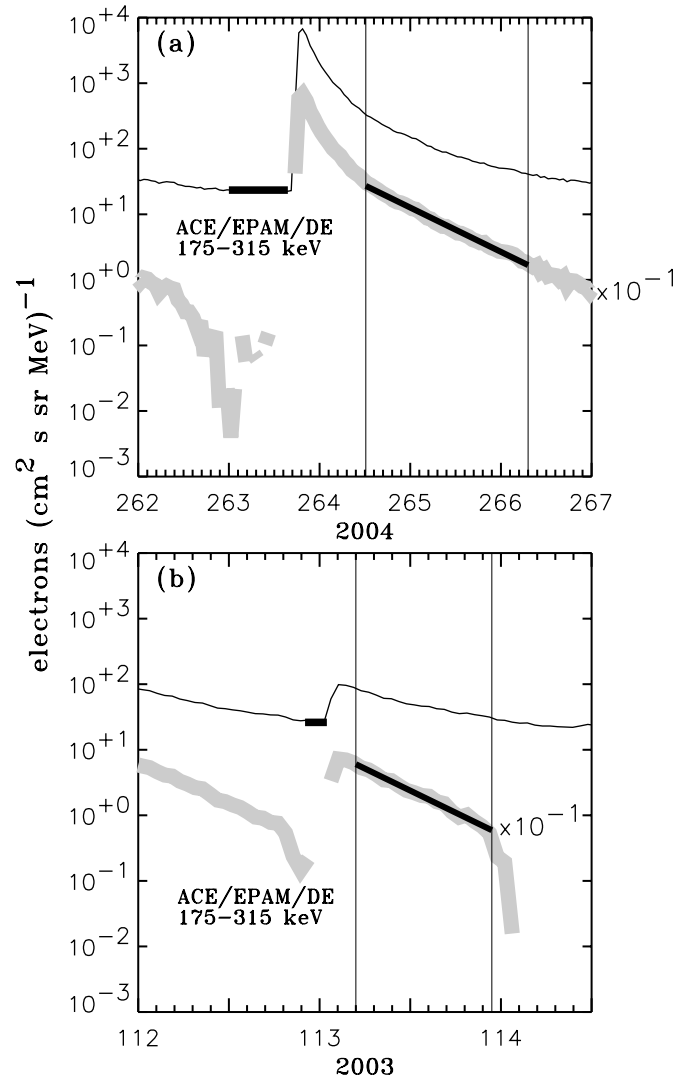


Figure 1. Time–intensity profile of two of the events selected. The thin black trace shows the 175–315 keV electron intensity as measured by DE telescope of EPAM on board *ACE*, whereas the thick gray trace shows the same intensities after subtraction of the averaged pre-event intensity (thick solid horizontal line). The gray traces have been scaled down by a factor of 10^{-1} . The two vertical thin lines delimit the time interval selected for the analysis of the decay phase. The thick black straight line is the result of the least-squares fit of a function $J \propto e^{-t/\tau}$.

For the event with onset on day 263 of 2004 (Figure 1(a)) we select the phase of the event with slow gradual exponential decay and neglect the first fast decay observed just after the peak of the event. For all the events showing this two-phase decay we have selected to study only the slower late decay. The onset of the selected time interval is visually chosen at that point where the time–intensity profile changes from a short decay-time constant to a longer decay-time constant. By contrast, the event with onset on day 113 of 2003 (Figure 1(b)) only shows a single characteristic decay rate and thus the selected time interval starts shortly after the peak intensity. The end of the selected time interval is marked by either the occurrence of a new intensity enhancement or when the pre-event subtracted intensities start fluctuating (but in any case the end time never reaches intensities below a factor of 1.05 above the pre-event intensity).

Whereas the selection of events is based exclusively on the highest energy channel of the DE telescope on board *ACE* and *Ulysses* (i.e., 175–315 keV), for all the selected

exponential declines we obtain the e -folding time τ using pre-event subtracted intensities from two differential energy channels, DE4:175–315 keV and DE2:53–103 keV (see below the criteria used to compute the decay rate when using the DE2 energy channel). We also compute the spectral index γ at the start (γ_1) and end (γ_2) times of the selected time intervals using three differential energy channels of the *ACE*/EPAM/DE and *Ulysses*/HI-SCALE/DE telescopes (DE2: 53–103 keV; DE3: 103–175 keV; DE4: 175–315 keV), as well as the solar wind speed V_{sw} averaged over the selected time interval using data from the solar wind experiment on *ACE* (McComas et al. 1998) or *Ulysses* (Bame et al. 1992). For each event we obtain at the two energy channels (DE2 and DE4) the peak intensity and the fluence computed as the integral of the electron intensities over time from the onset of the event until the time that either the intensity reaches the averaged pre-event intensity background or a new event starts.

Table 1 lists the events and decay time intervals selected from the *ACE*/EPAM/DE4 data set. From Columns 1–15 of Table 1 we list: (1) an index that numbers the event; (2) the time when the hourly averaged intensity of the event reaches its maximum t_{peak} (in units of day of the indicated year); (3) the event peak intensity J_{peak} (in units of particle $(cm^2 s sr MeV)^{-1}$); (4) the time interval over which we compute the event fluence Δt_{flu} (in units of day of the indicated year); (5) the event fluence F (in units of particle $(cm^2 sr MeV)^{-1}$); (6) the time interval used to compute the averaged pre-event intensity Δt_{bg} (in units of day of the indicated year); (7) the averaged pre-event intensity J_{bg} (in units of particle $(cm^2 s sr MeV)^{-1}$); (8) the time interval selected for the study of the decay phase of the event Δt_τ (in units of day of the indicated year); (9) the computed characteristic decay time τ (in units of hours); (10) the regression coefficient r obtained from the least-square fit to a function $J \propto e^{-t/\tau}$ over the time interval Δt_τ ; (11) the solar wind speed V_{sw} averaged over the time interval Δt_τ (in units of $km s^{-1}$); (12) the rate of increase or decrease of the solar wind speed dV_{sw}/dt over the time interval Δt_τ (in units of $km s^{-1} day^{-1}$); (13) the spectral index γ_1 measured at the start of the time interval Δt_τ ; (14) the spectral index γ_2 measured at the end of the time interval Δt_τ ; and (15) an indication of whether *Ulysses* registered an intensity increase in the electron channel *Ulysses*/HI-SCALE/DE4 that can be associated with the event observed by *ACE*/EPAM/DE4 (Y/N). The association is made in terms of (1) their concurrence (*Ulysses* intensity increase has to occur shortly ($\lesssim 12$ hr) after the *ACE* intensity increase) and (2) after a comprehensive survey of the main solar events occurring during the onset of the event at both spacecraft. A total of 168 events fulfilled our selection criteria. Note that Table 1 is published in its entirety in the electronic edition of the journal.

Table 2 lists the same parameters but using the energy channel *ACE*/EPAM/DE2 (53–103 keV). Note that the event selection criteria are based on the DE4 energy channel. From the list of events in Table 1 we select only those events in which (1) the 53–103 keV peak intensity is at least a factor of 1.2 above the pre-event intensity, (2) the exponential approximation $J \propto e^{-t/\tau}$ gives a good fit (regression coefficient $r > 0.9$) to the time profile of the particle intensities after pre-event intensity subtraction, and (3) the time interval over which we fit a function $J \propto e^{-t/\tau}$ is longer than 12 hr. When computing the decay rate τ at the energy channel *ACE*/EPAM/DE2, seven of the events selected using the energy channel *ACE*/EPAM/DE4 were rejected because of either their decay phases (after pre-event intensity subtraction) were shorter than 12 hr, the least-

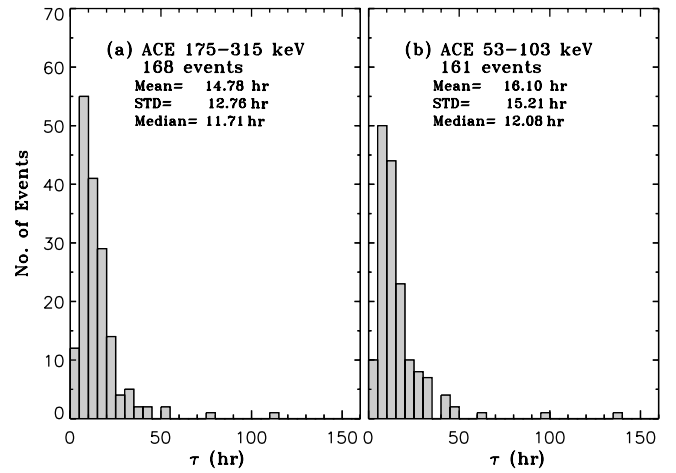


Figure 2. Decay rate distribution for the events listed in (a) Table 1 (*ACE*/EPAM/DE4) and (b) Table 2 (*ACE*/EPAM/DE2). The values of the mean, standard deviation (STD), and median for each distribution are indicated in the figure.

square fitting provided regression coefficients below 0.9, or the peak intensity of the event was below the factor of 1.2 times the pre-event intensity. Note that the time intervals used in the two energy channels DE4 and DE2 to compute τ can be slightly different according to the criteria described above. Table 2 is published in its entirety in the electronic edition of the journal.

Table 3 lists the same parameters but for the events selected using *Ulysses*/HI-SCALE/DE4 observations. A total of 55 decays met our selection criteria. Similarly, Table 4 lists the characteristics of the 54 decays for which we compute the decay rate at the energy range 53–103 keV from *Ulysses*/HI-SCALE/DE2 observations. The same selection criteria used for *ACE* observations were used to compute the *Ulysses* decay rates. Tables 3 and 4 are published in its entirety in the electronic edition of the journal.

4. *ACE* DECAY RATE RESULTS

In this section, we present the statistical analysis of the decay rates measured by *ACE*, paying attention to possible dependences between the decay rate τ and (1) the peak intensity of the SEP events, (2) the fluence of the SEP events, and (3) the energy of the electrons. We also investigate whether the peak intensity or the fluence of the events is correlated with either the duration of the decay or the characteristic decay time τ . For each analysis we check whether those events at *ACE* with or without an associated *Ulysses* intensity increase show different characteristics in their peak intensities, fluences, and decay rates τ .

Figure 2 shows the distribution of the values of the decay rate τ for the events of (a) the *ACE*/EPAM/DE4 data set (Table 1) and (b) the *ACE*/EPAM/DE2 data set (Table 2). Similar distributions are observed for both energy channels with slightly larger mean $\langle \tau \rangle$ and median M_τ values for the *ACE*/EPAM/DE2 than for the *ACE*/EPAM/DE4 distribution. Slightly larger values were found from the proton data set used by Kecskeméty et al. (2009). The average values of the decay rate $\langle \tau \rangle$ found by Kecskeméty et al. (2009) were $\langle \tau \rangle = 21.0$ hr for 0.5–4.6 MeV protons, $\langle \tau \rangle = 19.0$ hr for 15–25 MeV protons, and $\langle \tau \rangle = 16.6$ hr for 25–48 MeV protons. The higher the energy of the protons the lower the value of $\langle \tau \rangle$, but more similar to the values found for near-relativistic electrons.

Simultaneously or shortly after ($\lesssim 12$ hr) the onset of the events observed by *ACE*, we have studied whether *Ulysses*

Table 1
Parameters of the Events Measured by ACE/EPAM/DE4 and Selected for the Study of their Decay Phase

(1) No.	(2) t_{peak}^a	(3) J_{peak}^b	(4) Δt_{flu}^a	(5) F^c	(6) Δt_{bg}^a	(7) J_{bg}^b	(8) Δt_{τ}^a	(9) τ (hr)	(10) r	(11) V_{sw}^d	(12) dV_{sw}/dt^e	(13) γ_1	(14) γ_2	(15) I_{Uly}
1997														
1	307.646	5.96e1	307.400–308.230	1.09e6	307.200–307.450	2.90e1	307.650–308.230	6.49 ± 0.35	0.98	327.6 ± 4.4	4.5 ± 7.2	2.17 ± 0.15	1.74 ± 0.12	N
2	308.396	4.12e3	308.200–310.450	1.20e8	308.050–308.200	3.50e1	308.900–310.300	12.36 ± 0.21	1.00	352.7 ± 9.6	14.1 ± 3.2	2.38 ± 0.20	2.43 ± 0.09	N
3	310.729	3.41e4	310.450–315.010	2.21e9	310.300–310.450	7.14e1	313.510–315.010	12.13 ± 0.21	0.99	362.6 ± 12.1	-15.9 ± 3.9	1.83 ± 0.16	1.61 ± 0.18	Y
4	317.979	8.25e2	317.850–318.580	1.29e7	317.600–317.850	4.19e1	318.080–318.580	8.16 ± 0.75	0.96	346.6 ± 13.3	109.0 ± 15.5	1.91 ± 0.27	1.72 ± 0.26	N
1998														
5	27.021	2.57e2	26.850–27.780	4.02e6	26.700–26.900	2.79e1	27.250–27.750	4.51 ± 0.19	0.99	459.3 ± 11.0	36.9 ± 17.1	2.02 ± 0.17	1.79 ± 0.12	N
6	111.479	1.14e5	110.350–119.800	8.75e9	110.000–110.400	2.40e1	113.300–116.510	22.00 ± 0.11	1.00	419.3 ± 44.8	37.8 ± 3.4	1.81 ± 0.25	1.76 ± 0.19	Y
7	120.562	5.75e2	119.800–121.700	2.79e7	119.600–119.800	8.87e1	120.550–121.510	7.42 ± 0.32	0.98	376.5 ± 24.7	80.2 ± 7.6	3.11 ± 0.25	2.52 ± 0.11	N
8	122.688	9.35e3	122.550–123.900	2.92e8	122.470–122.570	3.70e2	122.800–123.900	7.38 ± 0.17	0.99	481.7 ± 36.2	-83.9 ± 15.7	1.95 ± 0.21	2.06 ± 0.19	N
9	126.354	3.13e4	126.310–127.850	3.70e8	126.270–126.320	9.13e1	126.700–127.850	8.80 ± 0.07	1.00	469.3 ± 17.1	29.0 ± 7.9	2.12 ± 0.17	2.10 ± 0.19	Y
10	129.521	7.68e2	129.120–131.250	5.09e7	128.850–129.150	5.60e1	130.300–131.100	11.34 ± 0.18	1.00	480.2 ± 20.4	-63.2 ± 14.6	1.86 ± 0.19	1.85 ± 0.16	Y

Notes.

^a Units are day of the year within the indicated year.

^b Units are particles $(\text{cm}^2 \text{ s sr MeV})^{-1}$.

^c Units are particles $(\text{cm}^2 \text{ sr MeV})^{-1}$.

^d Units are km s^{-1} .

^e Units are km (s day)^{-1} .

(This table is available in its entirety in a machine-readable form in the online journal. A portion is shown here for guidance regarding its form and content.)

Table 2
Parameters of the ACE/EPAM/DE2 Events

(1) No.	(2) t_{peak}^a	(3) J_{peak}^b	(4) Δt_{flu}^a	(5) F^c	(6) Δt_{bg}^a	(7) J_{bg}^b	(8) Δt_{τ}^a	(9) τ (hr)	(10) r	(11) V_{sw}^d	(12) dV_{sw}/dt^e	(13) γ_1	(14) γ_2	(15) I_{Uly}
1997														
1	307.646	7.34e2	307.300–308.230	2.16e7	307.200–307.400	1.28e2	307.700–308.200	8.05 ± 0.32	0.99	328.7 ± 3.4	−2.1 ± 7.1	2.21 ± 0.16	1.74 ± 0.09	N
2	308.396	4.94e4	308.210–310.500	1.63e9	308.050–308.200	2.81e2	308.700–310.400	14.69 ± 0.19	1.00	350.4 ± 12.7	20.0 ± 2.5	2.26 ± 0.22	2.36 ± 0.09	N
3	310.938	2.31e5	310.450–314.000	1.45e10	310.300–310.450	1.13e3	311.400–313.400	12.57 ± 0.11	1.00	399.3 ± 28.1	−43.1 ± 3.2	1.78 ± 0.19	1.85 ± 0.17	Y
4	317.979	6.98e3	317.850–318.560	1.11e8	317.600–317.850	2.10e2	318.060–318.560	6.69 ± 0.67	0.95	346.6 ± 13.3	109.0 ± 15.5	1.91 ± 0.27	1.72 ± 0.26	N
1998														
5	27.021	2.66e3	26.900–28.100	4.74e7	26.700–26.900	1.92e2	27.300–27.800	5.21 ± 0.16	0.99	458.3 ± 12.6	23.4 ± 25.4	2.02 ± 0.17	1.76 ± 0.07	N
6	111.479	5.21e5	110.350–117.600	4.99e10	110.000–110.400	1.23e2	113.300–116.600	21.59 ± 0.12	1.00	420.6 ± 44.9	37.2 ± 3.3	1.81 ± 0.25	1.77 ± 0.20	Y
7	120.604	2.12e4	119.700–121.900	8.76e8	119.600–119.800	1.35e3	120.600–121.400	5.46 ± 0.28	0.98	371.8 ± 19.9	73.0 ± 10.4	3.15 ± 0.23	2.45 ± 0.14	N
8	122.688	7.97e4	122.550–123.550	2.08e9	122.470–122.570	1.00e4	122.800–123.400	5.58 ± 0.20	0.99	503.5 ± 32.1	−184.0 ± 3.5	1.95 ± 0.21	2.01 ± 0.20	N
9	126.396	2.57e5	126.270–127.850	3.82e9	126.270–126.320	1.58e3	126.700–127.800	7.22 ± 0.10	1.00	468.7 ± 17.2	29.4 ± 8.5	2.12 ± 0.17	2.11 ± 0.17	Y
10	129.812	5.56e3	129.110–131.400	3.88e8	128.850–129.150	5.15e2	130.300–131.000	10.73 ± 0.30	0.99	482.3 ± 20.6	−69.3 ± 18.1	1.86 ± 0.19	2.11 ± 0.17	N

Notes.

^a Units are day of the year within the indicated year.

^b Units are particles (cm² s sr MeV)^{−1}.

^c Units are particles (cm² sr MeV)^{−1}.

^d Units are km s^{−1}.

^e Units are km (s day)^{−1}.

(This table is available in its entirety in a machine-readable form in the online journal. A portion is shown here for guidance regarding its form and content.)

Table 3
Parameters of the Events Observed by *Ulysses*/HI-SCALE/DE4 and Selected for the Study of their Decay Phase

(1) No.	(2) t_{peak}^a	(3) J_{peak}^b	(4) Δt_{flu}^a	(5) F^c	(6) Δt_{bg}^a	(7) J_{bg}^b	(8) Δt_{τ}^a	(9) τ (hr)	(10) r	(11) V_{sw}^d	(12) dV_{sw}/dt^e	(13) γ_1	(14) γ_2
1997													
1^U	314.521	6.48e1	311.200–325.010	1.14e7	310.500–311.200	3.56e1	315.100–321.000	103.92 ± 3.19	0.94	381.0 ± 14.7	0.2 ± 0.8	1.64 ± 0.20	1.57 ± 0.20
1998													
2^U	114.312	5.53e2	110.800–126.300	2.74e8	89.500–90.200	3.77e1	118.100–125.010	71.23 ± 0.44	1.00	428.7 ± 10.9	0.8 ± 0.4	2.12 ± 0.18	1.82 ± 0.17
3^U	159.938	1.17e2	155.900–164.800	2.32e7	155.500–155.900	3.27e1	160.010–162.010	25.51 ± 1.06	0.96	418.3 ± 13.8	-21.8 ± 1.3	1.90 ± 0.22	1.81 ± 0.23
4^U	244.062	1.29e2	236.500–262.000	7.50e7	236.000–236.500	3.36e1	248.000–260.000	89.29 ± 0.99	0.98	372.6 ± 20.8	-3.6 ± 0.3	1.69 ± 0.13	1.67 ± 0.15
5^U	333.521	1.31e2	331.000–338.750	2.19e7	330.500–331.000	4.67e1	335.510–338.521	32.86 ± 0.67	0.99	483.5 ± 14.6	3.2 ± 2.0	2.31 ± 0.16	2.22 ± 0.10
1999													
6^U	21.979	3.75e2	21.200–36.200	5.11e7	20.500–21.400	3.16e1	23.010–26.200	65.92 ± 1.17	0.99	452.1 ± 27.9	17.0 ± 2.9	1.66 ± 0.23	1.78 ± 0.19
7^U	156.312	1.34e2	153.200–167.010	4.06e7	152.500–153.200	3.20e1	157.010–163.010	59.62 ± 0.59	0.99	459.1 ± 14.2	2.3 ± 0.7	1.99 ± 0.19	1.82 ± 0.13
2000													
8^U	129.350	5.90e1	125.900–148.900	3.65e7	125.300–125.900	2.39e1	138.010–146.900	174.60 ± 3.91	0.95	372.8 ± 28.3	-9.6 ± 0.4	2.27 ± 0.13	2.03 ± 0.09
9^U	198.480	6.12e2	196.000–215.100	2.84e8	195.500–196.000	5.20e1	206.010–214.010	84.62 ± 1.48	0.97	357.1 ± 28.0	-10.5 ± 0.4	1.97 ± 0.19	1.98 ± 0.19
10^U	257.230	9.05e2	256.500–266.300	1.34e8	256.000–256.500	2.03e1	259.300–263.800	40.59 ± 0.29	1.00	415.7 ± 19.1	6.8 ± 1.3	2.25 ± 0.20	2.12 ± 0.11

Notes.

^a Units are day of the year within the indicated year.

^b Units are particles $(\text{cm}^2 \text{ s sr MeV})^{-1}$.

^c Units are particles $(\text{cm}^2 \text{ sr MeV})^{-1}$.

^d Units are km s^{-1} .

^e Units are km (s day)^{-1} .

(This table is available in its entirety in a machine-readable form in the online journal. A portion is shown here for guidance regarding its form and content.)

Table 4
Parameters of the Events Observed by *Ulysses*/HI-SCALE/DE2

(1) No.	(2) t_{peak}^a	(3) J_{peak}^b	(4) Δt_{flu}^a	(5) F^c	(6) Δt_{bg}^a	(7) J_{bg}^b	(8) Δt_{τ}^a	(9) τ (hr)	(10) r	(11) V_{sw}^d	(12) dV_{sw}/dt^e	(13) γ_1	(14) γ_2
1997													
1^U	314.479	4.26e2	310.600–328.010	1.04e8	310.500–311.200	1.29e2	315.100–325.010	93.67 ± 1.33	0.98	384.5 ± 15.2	2.0 ± 0.3	1.64 ± 0.20	1.58 ± 0.18
1998													
2^U	117.604	4.90e3	110.800–126.300	2.26e9	110.500–111.000	2.33e2	118.010–125.010	59.84 ± 0.42	1.00	428.3 ± 11.6	1.1 ± 0.4	2.14 ± 0.17	1.82 ± 0.17
3^U	159.979	1.12e3	155.900–164.800	2.27e8	155.500–155.900	1.50e2	160.010–162.010	26.83 ± 1.62	0.93	418.3 ± 13.8	-21.8 ± 1.3	1.90 ± 0.22	1.81 ± 0.23
4^U	241.062	1.72e3	236.500–263.050	9.65e8	236.000–236.500	1.38e2	248.010–260.010	114.21 ± 0.69	1.00	372.3 ± 20.3	-3.5 ± 0.3	1.92 ± 0.23	1.67 ± 0.15
5^U	333.521	1.71e3	331.000–340.010	4.15e8	330.500–331.000	4.03e2	335.510–340.010	45.18 ± 0.99	0.98	480.2 ± 16.7	-1.0 ± 1.2	2.31 ± 0.16	2.13 ± 0.11
1999													
6^U	21.979	2.46e3	21.200–30.510	3.47e8	20.500–21.400	1.14e2	23.010–26.200	82.77 ± 2.94	0.95	452.1 ± 27.9	17.0 ± 2.9	1.66 ± 0.23	1.78 ± 0.19
7^U	156.312	1.44e3	153.200–167.010	4.52e8	152.500–153.200	1.35e2	157.010–163.010	67.33 ± 0.74	0.99	459.1 ± 14.2	2.3 ± 0.7	1.99 ± 0.19	1.82 ± 0.13
8^U	127.100	9.86e2	125.900–151.400	7.76e8	125.300–125.900	8.39e1	138.010–143.900	156.21 ± 2.67	0.98	384.8 ± 26.9	-15.5 ± 0.3	2.27 ± 0.13	2.06 ± 0.11
2000													
9^U	200.980	4.03e3	196.000–210.200	1.87e9	195.500–196.000	6.45e2	204.010–210.010	47.62 ± 0.61	0.99	370.4 ± 20.1	6.7 ± 0.8	1.99 ± 0.21	1.99 ± 0.18
10^U	257.560	7.45e3	256.500–266.600	1.60e9	256.000–256.500	5.01e1	259.300–265.010	43.56 ± 0.62	0.99	420.4 ± 19.4	7.1 ± 0.8	2.25 ± 0.20	2.12 ± 0.12

Notes.

^a Units are day of the year within the indicated year.

^b Units are particles $(\text{cm}^2 \text{ s sr MeV})^{-1}$.

^c Units are particles $(\text{cm}^2 \text{ sr MeV})^{-1}$.

^d Units are km s^{-1} .

^e Units are km (s day)^{-1} .

(This table is available in its entirety in a machine-readable form in the online journal. A portion is shown here for guidance regarding its form and content.)

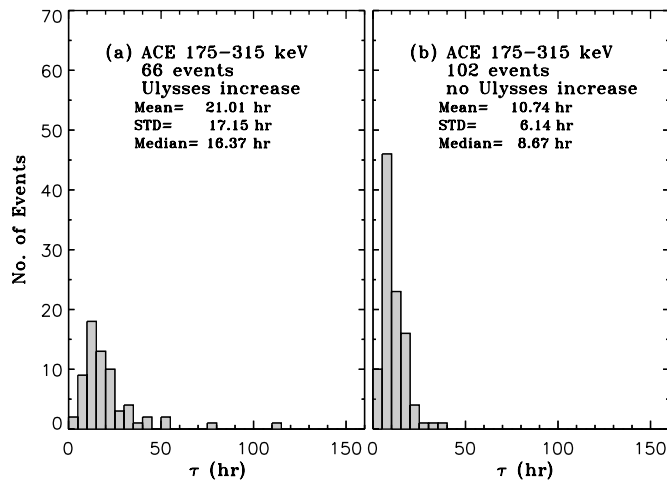


Figure 3. Decay rate distribution for the *ACE/EPAM/DE4* events (a) with and (b) without an associated electron intensity increase in the *Ulysses/Hi-SCALE/DE4* energy channel.

also detected an intensity enhancement. Among the 168 events selected from the *ACE/EPAM/DE4* data set, we distinguish those events where such an electron intensity increase was detected in the *Ulysses/Hi-SCALE/DE4* channel (66 events) from those where *Ulysses/Hi-SCALE/DE4* intensities did not show any enhancement (102 events). The last column of Table 1 identifies such events (Y when *Ulysses/Hi-SCALE/DE4* detected an intensity enhancement and N otherwise). Figure 3 shows the distributions of τ for the *ACE/EPAM/DE4* events (a) with and (b) without an associated *Ulysses* intensity increase. The events associated with an *Ulysses* intensity increase show a broader distribution with mean $\langle \tau \rangle$ and median M_τ values larger than those events without an associated *Ulysses* intensity increase. For the *ACE/EPAM/DE2* data set we obtain similar τ -distributions as those shown in Figure 3 with $\langle \tau \rangle = 19.65$ hr and $M_\tau = 14.52$ hr for those events with an associated *Ulysses/Hi-SCALE/DE2* intensity increase and $\langle \tau \rangle = 11.92$ hr and $M_\tau = 10.04$ hr for those events without an associated intensity increase at *Ulysses/Hi-SCALE/DE2*.

Figure 4 shows the dependence between the peak intensity J_{peak} and the fluence F of those events in the *ACE/EPAM/DE4* data set. The solid symbols in Figure 4 are used for those events with an associated *Ulysses/Hi-SCALE/DE4* intensity increase and the open symbols for those events without an *Ulysses/Hi-SCALE/DE4* intensity increase. In general, the events that have an associated *Ulysses* intensity increase show higher peak intensities and fluences. Considering all the events (with or without an associated *Ulysses* intensity increase), we find a clear correlation between the peak intensity J_{peak} and the event fluence F (indicated by the solid straight line and the equation in the bottom right corner of Figure 4). Our event selection criteria, based on the 175–315 keV electron peak intensity ($> 5 \times 10^1$ electrons $(\text{cm}^2 \text{ s sr MeV})^{-1}$) but not on the event fluence, produce a cutoff in the value of J_{peak} above this threshold. A series of events with low fluences but peak intensities above our threshold are observed at the lower left edge of Figure 4 (these events have been considered in the linear regression shown in Figure 4). For the events in the *ACE/EPAM/DE2* data set a similar correlation is found with $\log F = 4.45 + 1.05 \log J_{\text{peak}}$ and regression coefficient $r = 0.96$.

Figure 5 shows the decay rate τ as a function of (a) the peak intensity J_{peak} and (b) the event fluence F . In general, the events with an associated *Ulysses* intensity increase (solid

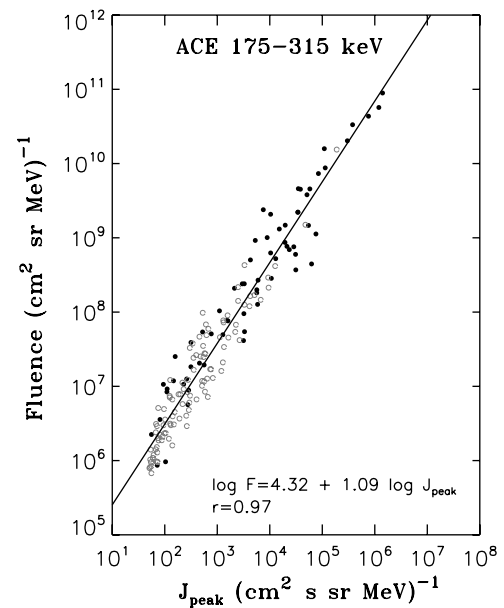


Figure 4. Correlation between event peak intensity J_{peak} and event fluence F for those events in the *ACE/EPAM/DE4* data set (Table 1). The black solid symbols are used for those events with an associated *Ulysses/Hi-SCALE/DE4* intensity increase and the open symbols for those events without an associated *Ulysses/Hi-SCALE/DE4* intensity increase. The black straight line results from a least-squares fit to all data points.

black symbols) show larger fluences, larger peak intensities, and larger decay rates τ than the events without an associated *Ulysses* intensity increase. Figure 5 shows that the low values of τ ($\tau < 10$ hr) extend over a broad range of peak intensities and fluences. It is only for the events with large peak intensities ($J_{\text{peak}} > 5 \times 10^4$ $(\text{cm}^2 \text{ s sr MeV})^{-1}$) and large fluences ($F > 2 \times 10^9$ $(\text{cm}^2 \text{ sr MeV})^{-1}$) that a trend to have large decay rates ($\tau > 10$ hr) can be found (we have plotted a dashed line in Figure 5 to guide the eye regarding this point).

In order to explore the possible correlation between the values of the decay rate τ and J_{peak} and F , we have computed (1) the duration of the exponential decay (i.e., the time interval Δt_τ used to compute τ for each event as listed in Column 8 of Table 1, and indicated by the two vertical thin lines in the examples shown in Figure 1), and (2) the duration of the decay of the event, Δt_{decay} , computed as the time interval from the peak intensity t_{peak} until the time when either the intensities reach the same level as the pre-event intensities or the decay is interrupted by a new event (i.e., the end time of the interval Δt_{flu} used to calculate the event fluence as listed in Column 4 of Table 1). Figure 6 shows the distributions of Δt_τ (left) and Δt_{decay} (right) for those events in the *ACE/EPAM/DE4* data set ((a) and (b)), distinguishing those events that have an associated intensity increase at *Ulysses/Hi-SCALE/DE4* ((c) and (d)) from those that do not have an associated *Ulysses* intensity increase ((e) and (f)). On average, the events that have an associated *Ulysses* intensity increase have longer decays as shown by the mean and median values in the respective panels of Figure 6. In contrast to the results shown in Figure 6(a), Kecskeméty et al. (2009) found bimodal distributions in the durations of the exponential decays selected for their study (see their Figure 3). Kecskeméty et al. (2009) selected those parts of the declines that could be reasonably fitted by an exponential; therefore, for some events, they included the two phases of the decay indicated by McKibben (1972; i.e., Phase 1 with a fast decay just after the peak intensity, and Phase 2 with a slower decay in the late phase of the event). Kecskeméty

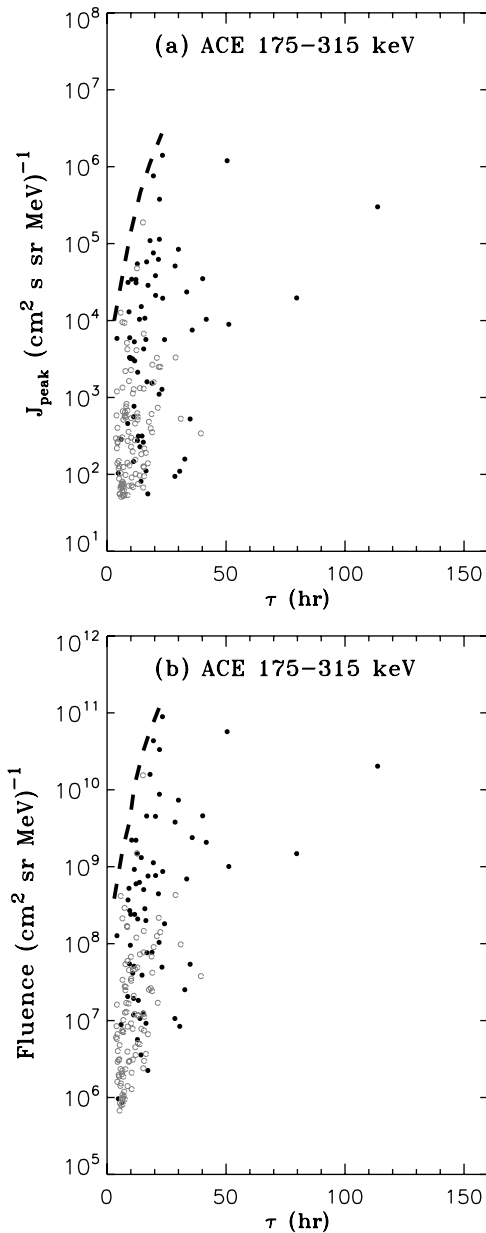


Figure 5. Scatterplots of the (a) peak intensity J_{peak} and (b) event fluence F vs. the decay time τ for the events of the ACE/EPAM/DE4 data set (Table 1). The black solid symbols are used for those events with an associated *Ulysses*/HI-SCALE/DE4 intensity increase and the open symbols for those events without an associated *Ulysses*/HI-SCALE/DE4 intensity increase. The dashed lines show that events with large peak intensities ($>5 \times 10^4 \text{ (cm}^2 \text{ s sr MeV)}^{-1}$) and large fluences ($>2 \times 10^9 \text{ (cm}^2 \text{ sr MeV)}^{-1}$) show long ($>10 \text{ hr}$) decay rates.

et al. (2009) recovered these two phases in the distributions of the exponential decay durations. By contrast, here we only use one phase for an event corresponding to either the late phase of the event (in the case that two phases are observed) or the decay with a constant rate observed just after the peak of the event. Therefore, the Δt_τ distributions of Figure 6 do not show such bimodal distributions.

Figure 7 shows the correlation between Δt_τ (left) and Δt_{decay} (right) with (a) Δt_{decay} and (b) Δt_τ , respectively; ((c) and (d)) τ ; ((e) and (f)) J_{peak} ; and ((g) and (h)) F . A clear cutoff is observed at the 12 hr value for Δt_τ because of the imposed selection criteria. The events that have an associated *Ulysses* intensity increase (solid black symbols) clearly show large values of Δt_τ , Δt_{decay} , τ , J_{peak} , and F , suggesting that large and intense events

are required to be observed by both spacecraft. As expected, the events with long decays (either Δt_τ or Δt_{decay}) tend to have large fluences, whereas events with large J_{peak} tend to have longer decays; however, there is no clear proportionality law between J_{peak} and either Δt_τ or Δt_{decay} , or between F and either Δt_τ or Δt_{decay} (see also Figure 5). Figure 7(c) shows some correlation between Δt_τ and τ , also found by Kecskeméty et al. (2009, see their Figure 5). A linear fit to the data in Figure 7(c) yields $\tau = 5.21 + 0.29\Delta t_\tau$ (hr) with a regression coefficient $r = 0.85$. A certain degree of correlation can also be found between Δt_{decay} and τ , but the dispersion is larger than in the case of τ versus Δt_τ . A linear fit to the data in Figure 7(d) yields $\tau = 4.59 + 0.16\Delta t_{\text{decay}}$ (hr) with a regression coefficient $r = 0.81$. In general, the longer the τ the longer the decay.

From the decay rates computed for the events selected from ACE/EPAM/DE4 (Table 1) and ACE/EPAM/DE2 (Table 2) we can compare the values of τ obtained at the two energy ranges 175–315 keV (τ_{DE4}) and 53–103 keV (τ_{DE2}), respectively. Figure 8 shows the distribution of the ratio $\tau_{\text{DE2}}/\tau_{\text{DE4}}$ for the 161 events with computed decay rates at both energy channels. Within the error bars of τ , most of the events show similar values of τ_{DE2} and τ_{DE4} , i.e., there is no strong energy dependence in the decay rates within our energy range. This result suggests an invariance of the spectra during the decay phase of the near-relativistic electron events. Nevertheless, the $\tau_{\text{DE2}}/\tau_{\text{DE4}}$ distribution of Figure 8 shows a tail of events (45 out of the 161 events) with $\tau_{\text{DE2}}/\tau_{\text{DE4}} > 1.2$ suggesting that 53–103 keV electron intensities may decrease slower than the 175–315 keV electron intensities (in contrast with only 14 events out of the 161 with $\tau_{\text{DE2}}/\tau_{\text{DE4}} < 0.8$). If this is interpreted in terms of diffusion, that would imply that lower energy electrons have a smaller mean free path than higher energy electrons; however this is opposite to the energy dependence of the electron mean free paths obtained by transport models (e.g., Dröge 2000). If this is interpreted in terms of the electrons being confined in an expanding volume between the increasing magnetic field near the Sun and traveling interplanetary magnetic field structures beyond the observer, the faster the electrons the more likely they are to leak or escape from this expanding volume and hence a faster decay. If the tail of events with $\tau_{\text{DE2}}/\tau_{\text{DE4}} > 1.2$ is interpreted in terms of adiabatic cooling, it would imply that in a given energy range, the electron intensity decreases faster the higher the energy of the electrons which depends on the energy distribution of electron intensities (see Section 7).

Kecskeméty et al. (2009) found that in the energy range 4.6–48 MeV, a 56% of the decays showed decay rates τ that are independent of the proton energy (indicating that the proton spectrum remains unchanged during the decay), a 37% of the decays where τ decreases with the proton energy (indicating that the spectrum becomes softer during the decay), and only a 7% of the decays where τ increased with the energy. The decays where τ decreases with the proton energy were interpreted as a result of the energy dependence of the diffusion processes, in agreement with the energy dependence assumed for the proton mean free paths (e.g., Dröge 2000).

5. LONGITUDINAL DEPENDENCE OF THE ACE DECAY RATES

As described in Section 1, the first studies of high-energy solar proton events showed a dependence between the longitude of the solar phenomena associated with the origin of the event and the time–intensity profile observed during their decay (Burlaga 1967). Events associated with western solar flares

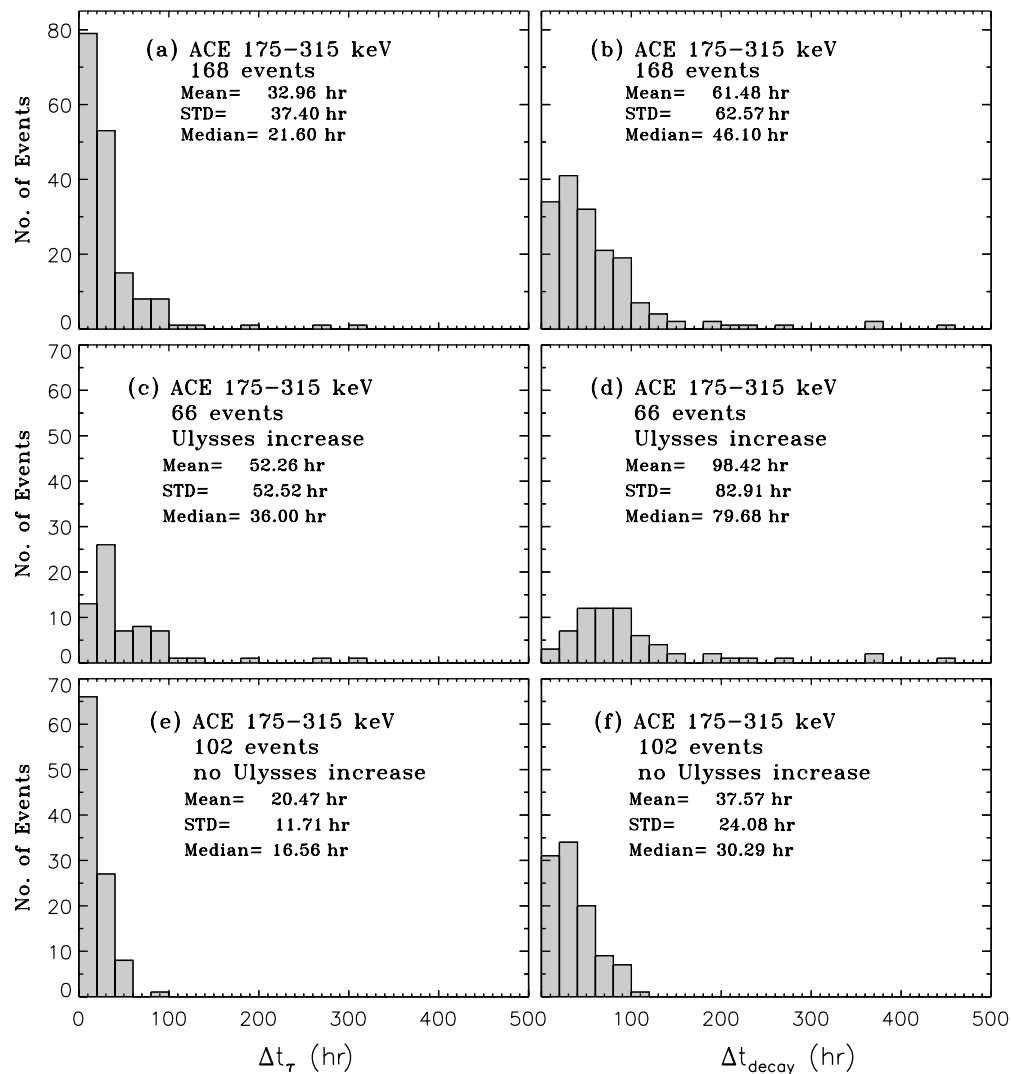


Figure 6. Distributions of the exponential decay time interval Δt_τ (left) and the total duration of the event decay Δt_{decay} (right) for (a) and (b) those events of the *ACE/EPAM/DE4* data set listed in Table 1, and for those events (c) and (d) with and (e) and (f) without an associated *Ulysses/HI-SCALE/DE4* intensity increase.

have time–intensity profiles with a strong peak followed by a period of a power-law decay just after the maximum and then an exponential decay at late times. By contrast, events associated with eastern flares have a maximum intensity less marked and the entire decay follows an exponential decay (Burlaga 1967). In this section, we analyze whether the dependence between the longitude of the parent solar event and the time–intensity profile of the decay phase is also observed in near-relativistic electron events. We also analyze whether the decay rate τ is correlated with the longitude of the parent solar event as expected from the corotation of the flux tubes moving over the spacecraft as discussed in Section 2 (see also McCracken 1971).

For 153 events out of the 168 events of Table 1, we have identified the solar phenomena (either solar flare and/or coronal mass ejection (CME)) temporally associated with the origin of the SEP event. The associations between SEP event and solar origin were based on the works of Cane et al. (2006), Cliver et al. (2005), Lario et al. (2000), reports on the *SOHO/LASCO* CME catalog compiled by Yashiro et al. (2004)¹, and Solar Geophysical Data reports². Table 5 shows for each event the parameters of either the solar flare ($H\alpha$ location, soft X-ray

class, and time of the maximum 1–8 Å X-ray emission) or the CME associated with the origin of the near-relativistic electron event. The association of events with longitudes beyond either the west ($> +90^\circ$) or the east ($< -90^\circ$) limb is based on either the tracking of active regions during their transit over the visible solar disk (Lario et al. 2000; Cliver et al. 2005; Cane et al. 2006) or comments included in the *SOHO/LASCO* CME catalog³. For 12 events the only possible solar event associated with the origin of the near-relativistic electron event was a CME with indications of being associated with a backside event (indicated by W+ in Table 5). We have also identified in Table 5 whether the time–intensity profile of each event shows only one phase during its decay as the event shown in Figure 1(b) (type 1), two different phases as the event shown in Figure 1(a) (type 2), a peak before the exponential decay associated with the passage of an interplanetary transient shock in the form of an energetic storm particle (ESP) event (type 3), or whether the time–intensity profile was disturbed by the presence of interplanetary structures (either SIRs, ICMEs, or shocks; type 4). For six events we were not able to classify the time–intensity profile in any of these groups (type –9).

¹ http://cdaw.gsfc.nasa.gov/CME_list/

² <http://www.ngdc.noaa.gov>

³ <ftp://lasco6.nascom.nasa.gov/pub/lasco/status>

Table 5
Solar Origin and Type of Decay for the Events of the *ACE*/EPAM/DE4 Data Set

(1) Event	(2) Solar Event ^a	(3) Type ^b	(4) Delay ^c	(1) Event	(2) Solar Event ^a	(3) Type ^b	(4) Delay ^c	(1) Event	(2) Solar Event ^a	(3) Type ^b	(4) Delay ^c
1	S20W15 M1 1997/307/09:10	1	0.09	2	S14W33 X2 1997/308/05:58	2	12.09	3	S18W63 X9 1997/310/11:55	2	66.74
4	~W100 ^d 1997/317/22:25	2	12.42	5	S17W55 C5 1998/026/22:35	2	5.50	6	S43W90 ^e M1 1998/110/10:00	2	43.70
7	S18E20 M6 1998/119/16:37	4	-0.29	8	S15W15 X1 1998/122/13:42	1	2.69	9	S11W65 X2 1998/126/08:09	2	8.30
10	W103 ^d M7 1998/129/03:40	-9	18.70	11	W+ ^f 1998/131/21:55	1	0.53	12	S23W83 C7 1998/147/13:23	1	-0.09
13	W+ ^f 1998/150/23:28	1	4.10	14	~W103 ^d M1 1998/167/18:42	4	39.81	15	N30E07 X1 1998/236/22:05	3	26.90

Notes.

^a Solar event most likely related to the origin of the near-relativistic electron event at *ACE*. For flares, H α location and time of the 1–8 Å X-ray peak emission (in format year/day/hour:minute).

^b Type of SEP decay: 1, only one decay phase; 2, two phases; 3, after a ESP event; 4, profile disturbed by unrelated interplanetary structures; -9, unclassified.

^c Delay between t_{peak} and the onset of the time interval Δt_r (units are hours).

^d Based on Table 1 of Lario et al. (2000).

^e Based on Table 1 of Cane et al. (2006).

^f Based on the occurrence of a CME as reported on http://cdaw.gsfc.nasa.gov/CME_list/ and/or <ftp://lasco6.nascom.nasa.gov/pub/lasco/status>.

^g Based on the association made by Simnett et al. (2002).

^h Based on the association made by Cliver et al. (2005).

(This table is available in its entirety in a machine-readable form in the online journal. A portion is shown here for guidance regarding its form and content.)

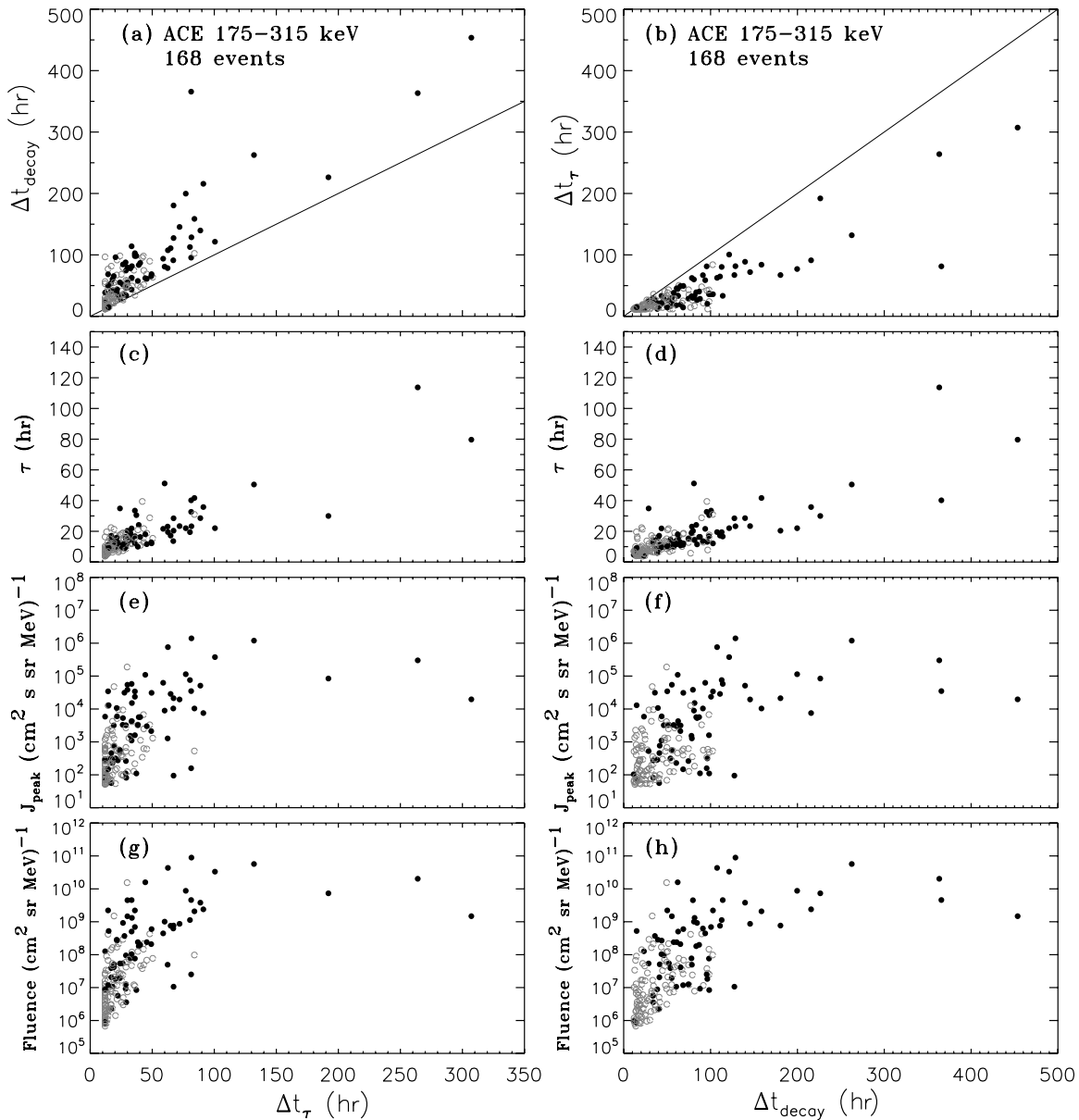


Figure 7. Left: correlation between Δt_τ and (a) Δt_{decay} , (c) τ , (e) J_{peak} , and (g) F . Right: correlation between Δt_{decay} and (b) Δt_τ , (d) τ , (f) J_{peak} , and (h) F for the events in the ACE/EPAM/DE4 data set. The black solid symbols are used for those events with an associated *Ulysses*/HI-SCALE/DE4 intensity increase and the open symbols for those events without an associated *Ulysses*/HI-SCALE/DE4 intensity increase.

We also list in Table 5 the delay between the time of the peak of the event t_{peak} (Column 2 in Table 1) and the start time of the period selected to compute the decay rate (i.e., the first time of the interval Δt_τ indicated in Column 8 of Table 1). Note that t_{peak} was automatically selected over the hourly averaged electron intensities measured during each event, whereas both the period Δt_τ and the type of decay of the event were visually selected by looking at the time–intensity profile. For that reason, the delays listed in Table 5 are not exact integers. For the same reason, any single-point irregularity in the time–intensity profile during the decay may lead to small negative values of this delay when the peak intensity occurs within the hour when the interval Δt_τ starts. Note that Table 5 is published in its entirety in the electronic edition of the journal.

Figure 9 shows the distribution of the values of the delay between t_{peak} and the start of the decay Δt_τ (a) for all the events in the ACE/EPAM/DE4 data set (Table 1), (b) for those events

in which only one decay phase is observed (type 1), and (c) for those events in which two decay phases can be distinguished. As expected, for type 1 events, the time interval Δt_τ starts shortly after the peak t_{peak} , whereas for type 2 events, there is a delay of several hours between t_{peak} and the start of Δt_τ . Since the selection of the decay phases was done in an event-by-event basis, regardless of the observation of heliospheric reservoirs, these results are not directly comparable to those of Lario (2010) regarding when the reservoirs were observed with respect to the peak intensity of the events.

Figure 10 shows the decay rate τ of the events as a function of the longitude of the associated flare. The different symbols indicate the type of time–intensity profile. The events associated with backside solar phenomena (W+) are plotted at W175°. The events 62 and 85 with extremely long decay rates remain outside the domain of the figure. Figure 10 shows that, in general, (1) the events showing two decay phases (black solid symbols) are

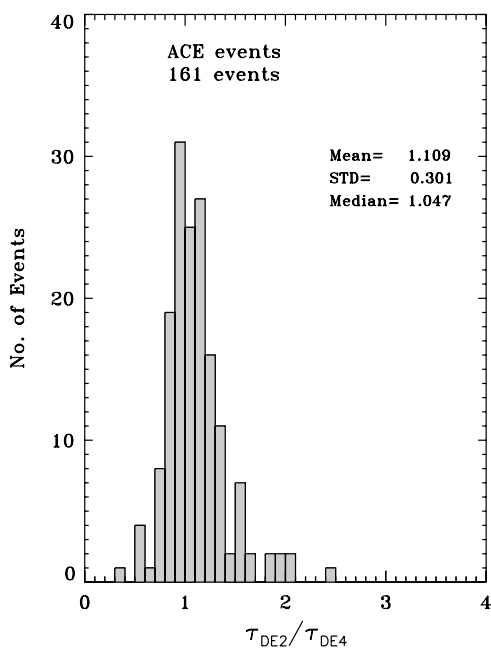


Figure 8. Distribution of the ratio between the decay rates from the data sets ACE/EPAM/DE2 (τ_{DE2} ; Table 2) and ACE/EPAM/DE4 (τ_{DE4} ; Table 1).

generated from well-connected longitudes (Burlaga 1967), (2) the events showing an ESP event (plus symbols) are generated from longitudes close to the Sun–Earth line, and (3) events showing only one decay phase (gray solid symbols) are mostly generated from poorly-connected longitudes (either at the west or the east from the nominal well-connected longitudes). The distribution of the event longitudes (regardless of the type of the event and excluding the W+ events) has a mean longitude of $35^{\circ}8$ and median of 39° . The distribution of longitudes (excluding the W+ events) for type 2 events has a mean longitude of $61^{\circ}6$ and median of 62° , whereas for the type 1 events the mean longitude is $17^{\circ}5$ and median 17° , and the type 3 events the mean value is $1^{\circ}5$ and median -7° .

Figure 10 shows that there is no clear dependence between τ and the longitude of the associated solar flare. The exception is that for nominal well-connected longitudes ($50^{\circ}W-70^{\circ}W$) the low values (<15 hr) of τ are more abundant than for other poorly-connected longitudes. Such independence of τ with respect to longitude, including also a larger amount of low values of τ for well-connected longitudes, was also observed by Kecskeméty et al. (2009, see their Figure 11).

The factors that may regulate a dependence between τ and the longitude of the parent solar event are (1) the longitudinal profile of the source injecting particles into the different flux tubes that move over the observer during the decay phase of the event, (2) the time profile of the particle injection in each flux tube in the case of long-lasting sources, and (3) the particle transport conditions within each flux tube. If the injection of particles is very focalized around the flare site, the event will only be observed from well-connected spacecraft and with a fast decay because the number of populated flux tubes will be small. If the injection of particles is extended over a broad range of longitudes, the decay may last longer and thus be observed by poorly-connected spacecraft. Hence the low τ values for well-connected events. McCracken (1971) showed that the decay time may be a function of the position of the observer relative to the centroid of the SEP population injected by the flare. As seen from the Earth, events generated by eastern flares may show

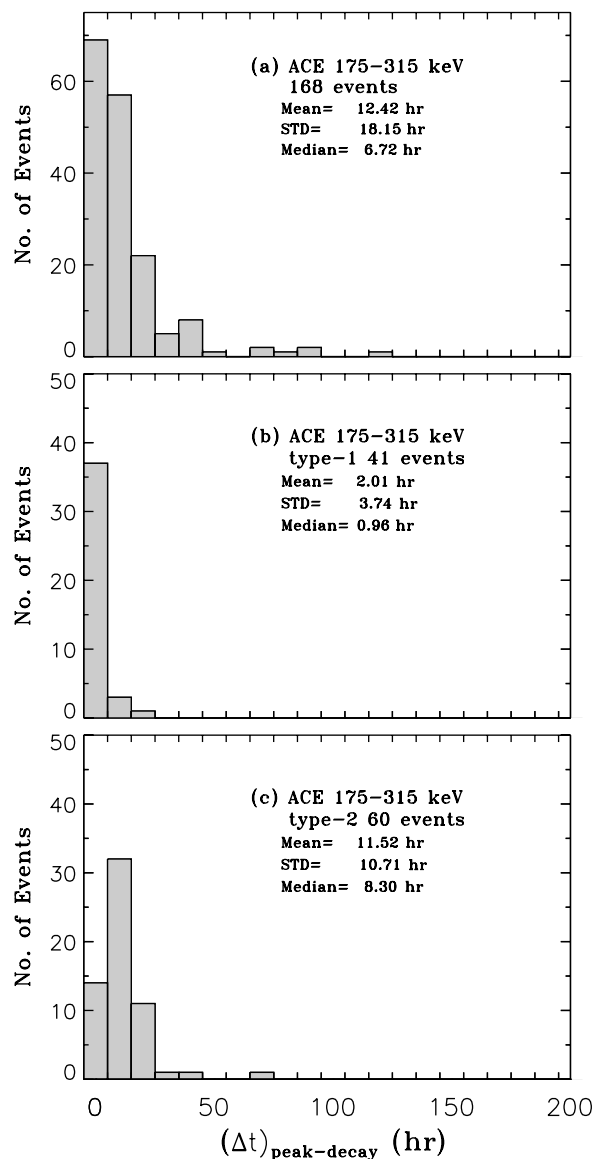


Figure 9. Distribution of the delay between t_{peak} and the onset of the time interval Δt_{τ} for (a) all the events in the ACE/EPAM/DE4 data set; (b) for those events with one phase during their decay (type 1); and (c) for those events with two phases during their decay (type 2).

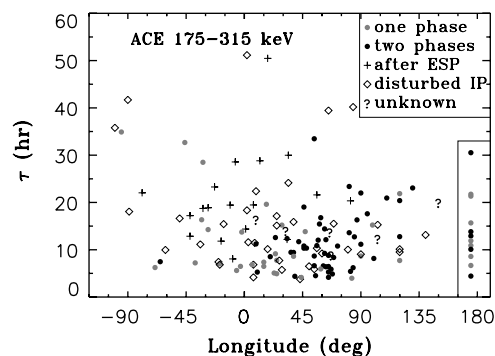


Figure 10. Distribution of the decay rates τ of the ACE/EPAM/DE4 data set as a function of the longitude of the associated solar flare. Events showing only one phase in their decay are represented by gray solid symbols, events with two phases by black solid symbols, events with decays occurring after the observation of an electron ESP event by plus symbols, events disturbed by interplanetary structures by open diamonds, and events with unclassified decay profile by question marks.

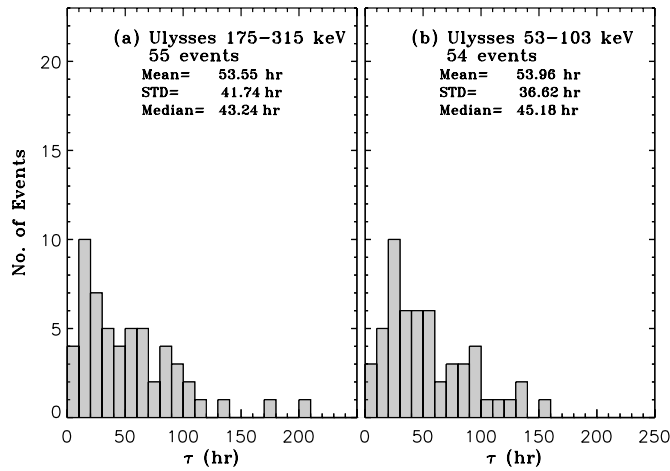


Figure 11. Decay rate distribution for (a) the events listed in Table 3 and measured by *Ulysses*/HI-SCALE/DE4, and (b) the events listed in Table 4 and measured by *Ulysses*/HI-SCALE/DE2. The values of the mean, standard deviation (STD), and median for each distribution are indicated in the figure.

slow decays because of the corotation effect of the flux tubes populated by SEPs whereas events generated by western flares may show faster decays (see Figure 8 of McCracken 1971). Figure 10 shows that whereas far-eastern events may have long decay rates, long τ events can be observed from all longitudes.

6. ULYSSES DECAY RATE RESULTS

The description of the results obtained from the analysis of the *Ulysses* decay rates follows the same approach as that used to describe the results obtained from *ACE* (Section 4). Figure 11 shows the distributions of the decay rates τ for (a) the events listed in Table 3 corresponding to the *Ulysses*/HI-SCALE/DE4 data set, and (b) the events listed in Table 4 corresponding to the *Ulysses*/HI-SCALE/DE2 data set. Similarly to the decay rate distributions obtained from *ACE* (Figure 2), the distributions obtained at low (DE2) and high (DE4) energies at *Ulysses* are very similar. However, the *Ulysses* distributions are broader (more disperse) than those obtained for *ACE*. Larger values of τ are more commonly observed at *Ulysses* than at *ACE*. The comparison of the decay rate for those events observed in common by *ACE* and *Ulysses* is deferred to Section 8.

Comparison of *Ulysses* and *ACE* near-relativistic electron intensities shows that whereas *ACE* detects many more electron intensity increases than *Ulysses*, most of the *Ulysses* increases can be associated with either single *ACE* events or a sequence of events at *ACE* that merge as a single event at *Ulysses* (Simnett 2001; Lario 2010). Therefore, we will not distinguish here those events at *Ulysses* that have an associated intensity increase at *ACE* from those that do not have an intensity increase at *ACE* as done for the case of 1 AU observations in Figure 3. A notable exception was the event observed by *Ulysses* on day 210 of 2007 (event 55^U in Table 3) when *Ulysses* was at heliocentric radial distance $R = 1.41$ AU, heliographic latitude $\Lambda = -8^\circ$, and heliolongitude with respect to the Earth $\Phi = 30^\circ$; and *ACE* did not detect any associated electron intensity increase.

Figure 12 shows the correlation between J_{peak} and F for those events from the *Ulysses*/HI-SCALE/DE4 data set. As expected, the higher the peak flux the higher the fluence; however, the correlation coefficient is smaller than that found in the case of *ACE* (Figure 4). Similarly to Figure 4, and because of our selection criteria based on a J_{peak} threshold, a few events with

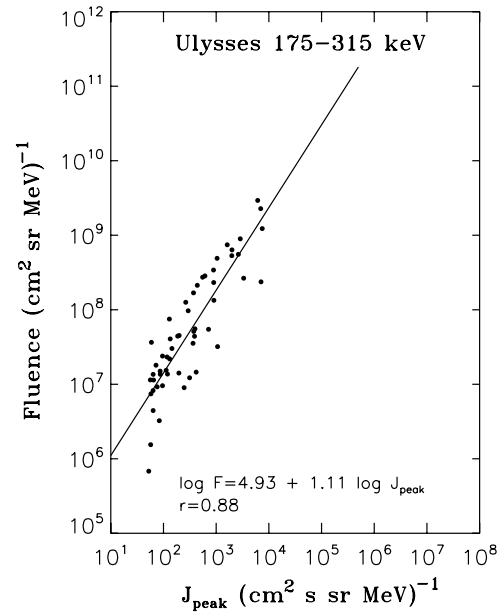


Figure 12. Correlation between event peak intensity J_{peak} and event fluence F for those events in the *Ulysses*/HI-SCALE/DE4 data set (Table 3). The black straight line results from a least-squares fitting to the data points.

$J_{\text{peak}} > 5 \times 10^1$ electrons $(\text{cm}^2 \text{ s sr MeV})^{-1}$ but low fluences appear in the lower left edge of Figure 12 that depart from the correlation law indicated by the straight line in Figure 12 (these events have indeed been considered in the linear regression shown in Figure 12). For the *Ulysses*/HI-SCALE/DE2 data set a similar correlation is found with $\log F = 5.31 + 0.98 \log J_{\text{peak}}$ and $r = 0.87$.

Figure 13 shows (a) the event peak intensities J_{peak} and (b) event fluences F as a function of the decay rate τ . No correlation can be inferred from Figure 13 except for the fact that low fluence events ($F < 8.0 \times 10^6$ $(\text{cm}^2 \text{ sr MeV})^{-1}$) do not have long decay rates ($\tau < 25$ hr), and events with large fluences ($F > 3.0 \times 10^8$ $(\text{cm}^2 \text{ sr MeV})^{-1}$) tend to have long decay rates ($\tau > 24$ hr).

Figure 14 shows the distributions of (a) the duration of the exponential decay Δt_τ (listed in Column 8 of Table 3) and (b) the duration of the decay phase Δt_{decay} (computed in the same way as done for *ACE* observations; i.e., the time interval from the peak of the event to the end of the time interval over which the event fluence is computed). Note that the time of the maximum intensity at *Ulysses* is less marked than at *ACE* especially for the events observed at large heliocentric distances (e.g., see Figure 9 in Lario et al. 2000). The decays at *Ulysses* are much longer than those observed at *ACE* (Figure 6), reaching extreme values for Δt_{decay} of ~ 20 days as a maximum (like in the intense events on days 227 (event 23^U) and 271 (event 24^U) of 2001 with *Ulysses* at $R = 1.65$ AU, $\Lambda = +64^\circ$ and at $R = 1.90$ AU, $\Lambda = +78^\circ$, respectively). The mean values of both Δt_τ and Δt_{decay} are much longer than those observed for *ACE* (1.4 days versus 4.1 days for Δt_τ , and 2.5 days versus 7.4 days for Δt_{decay}), whereas this comparison is more similar for those *ACE* events that have an associated increase at *Ulysses* (2.2 versus 4.1 days for Δt_τ and 4.1 days versus 7.4 days for Δt_{decay}). A few events at *ACE* with an associated intensity increase at *Ulysses* (Figure 6(c)) show long Δt_τ similar to those observed at *Ulysses*. As expected, the Δt_{decay} distribution at *Ulysses* (Figure 14(b)) is more spread out than the Δt_τ distribution. Since only a portion of the event decline corresponds to the late phase of

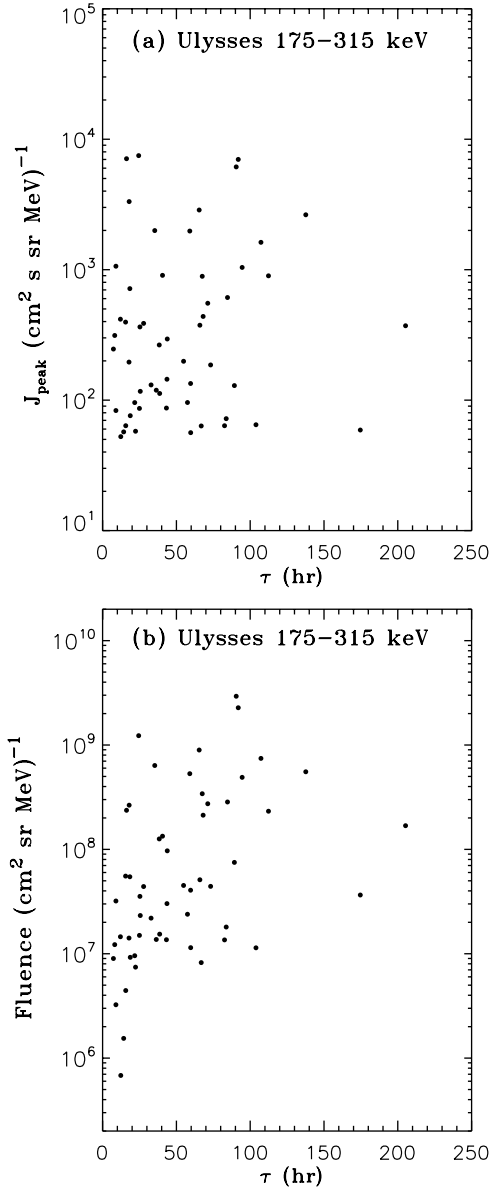


Figure 13. Scatterplots of (a) the peak intensity J_{peak} and (b) the event fluence F vs. the decay time τ for the events in the *Ulysses*/HI-SCALE/DE4 data set (Table 3).

the decay, the mean and median values of Δt_{decay} are larger than the corresponding values of the Δt_{τ} distribution.

Figure 15 shows the possible correlations between Δt_{τ} (left) and Δt_{decay} (right) with (a) Δt_{decay} and (b) Δt_{τ} , respectively; ((c) and (d)) τ ; ((e) and (f)) J_{peak} ; and ((g) and (h)) F . As expected, the longer the decay (either Δt_{τ} or Δt_{decay}) the longer the decay rate τ . Similarly, the longer the decay the higher the fluence of the event, although no significant proportionality law can be inferred from Figures 15(g) and (h). However, no correlation is found between J_{peak} and either Δt_{τ} , Δt_{decay} or τ (Figures 15(e) and (f); see also Figure 13). It is worth mentioning that the dispersion of Δt_{τ} and Δt_{decay} values in each one of the panels of Figure 15 is larger than those observed for *ACE* in Figure 7.

Figure 16 shows the distribution of the ratio between the decay rate obtained from the *Ulysses*/HI-SCALE/DE4 (Table 3) and the *Ulysses*/HI-SCALE/DE2 (Table 4) data sets. Within the error bars most of the events show similar values between τ_{DE2} and τ_{DE4} but a slight tendency for events with $\tau_{\text{DE2}} > \tau_{\text{DE4}}$

is shown in Figure 16. This result suggests either an energy independence on the decay rate (for most of the events and within our energy range) or slightly longer decays for low energies (19 events out of the 54 events had $\tau_{\text{DE2}}/\tau_{\text{DE4}} > 1.2$, whereas only three events showed $\tau_{\text{DE2}}/\tau_{\text{DE4}} < 0.8$).

Since the dependence usually found at 1 AU between the time–intensity profile and the longitude of the parent solar event is not found for those events observed at larger heliocentric distances (e.g., Lario et al. 2000) and owing to the fact that multiple SEP injections usually merge to form a single SEP event at *Ulysses* (Lario et al. 2000), here we do not perform any longitudinal study of the decay rates at *Ulysses* as done for *ACE*. Those events concurrently observed at *ACE* and *Ulysses* with evidence of being dominated by only one single SEP injection will be studied in Section 8.

7. SOLAR WIND CONVECTION AND ADIABATIC DECELERATION EFFECTS ON THE DECAY PHASE OF THE EVENTS

As commented in Section 2, possible mechanisms controlling the decay rate of SEP events that can be easily examined from our data set include solar wind convection and adiabatic deceleration. Considering only the convective motion of the particles with the solar wind, one may expect that the decay rates τ decrease with increasing solar wind speed V_{sw} (Kecskeméty et al. 2009). Considering only the adiabatic deceleration effect, one should expect τ to decrease with the increase of the spectral index γ , in the sense that, since particle energy decreases with time, the decrease in intensities is more pronounced as the energy spectrum steepens (Lee 2000).

Forman (1970) presented a simple model to reproduce the exponential decay observed in SEP events. She used a transport equation that follows from a scattering mechanism comoving with the solar wind in the case of a spherical solar wind, neglecting the focusing effect and assuming isotropic particle distributions dominated by convection effects with the approximation of small spatial gradients. Forman (1970) obtained the following approximate equation for the intensity decay rate:

$$\tau_{\text{theor}} = \frac{3}{(2 + \alpha\gamma)} \frac{R}{2V_{\text{sw}}}, \quad (1)$$

where R is the heliocentric radial distance, V_{sw} is the solar wind speed, γ is the exponent of the SEP power-law energy spectrum, and $\alpha = (T + 2mc^2)/(T + mc^2)$ with T being the kinetic energy of the particles. Roelof (1975) showed that in the case of scatter-free propagation and collimated convection with the additional assumption of particle scattering at a region beyond 1 AU (~ 2 AU) similar values for the decay rate can be obtained. Collimated convection was used to describe the large-scale transport of the energetic particles in which the net transverse motion is that of the field line itself (comoving with the solar wind) and the parallel motion is determined by the conditions along the field line. Forman (1970) noted that, for an observer at $R = 1$ AU, the decay time τ_{theor} given by Equation (1) is fairly uniform from event to event as V_{sw} and γ are not highly variable.

In this section, we compare the values obtained for τ with V_{sw} , γ , and the theoretical expression of τ_{theor} . The spectral index γ is obtained from the average of γ_1 and γ_2 computed at the start and end times of the interval Δt_{τ} . Following Kecskeméty et al. (2009) we distinguish those decay periods during which the solar wind speed (1) increased ($dV_{\text{sw}}/dt > 0$), (2) decreased

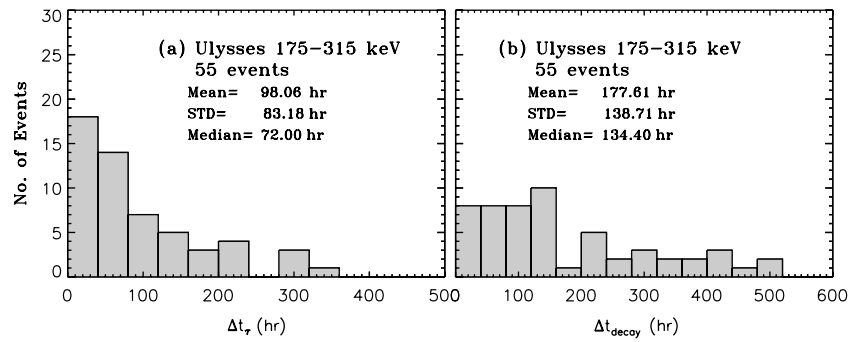


Figure 14. Distributions of (a) the exponential decay time interval Δt_τ and (b) the total duration of the event decay Δt_{decay} for those events of the *Ulysses*/HI-SCALE/DE4 data set listed in Table 3.

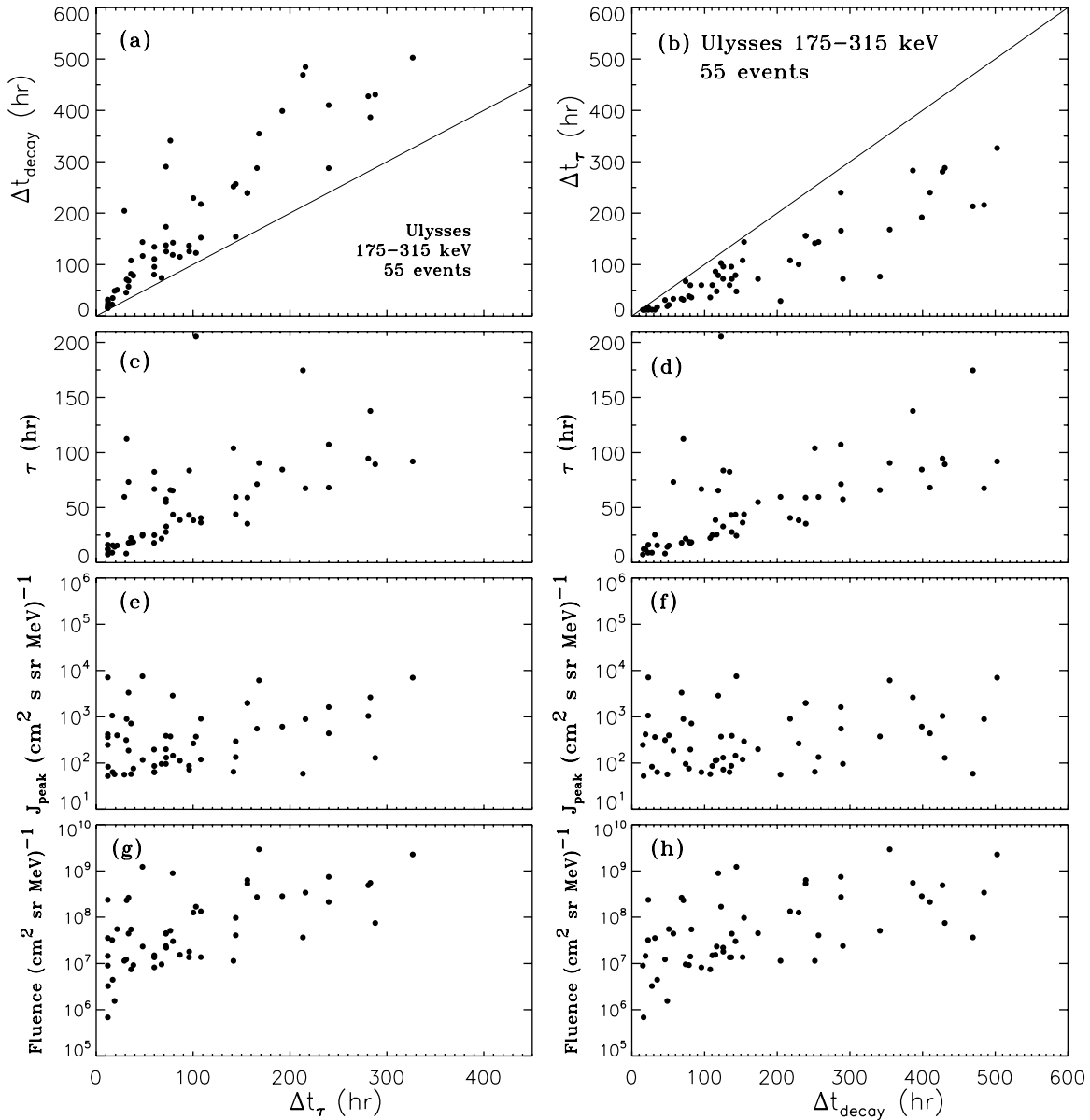


Figure 15. Left: correlation between Δt_τ and (a) Δt_{decay} , (c) τ , (e) J_{peak} , and (g) F . Right: correlation between Δt_{decay} and (b) Δt_τ , (d) τ , (f) J_{peak} , and (h) F for the events in the *Ulysses*/HI-SCALE/DE4 data set.

($dV_{\text{sw}}/dt < 0$), or (3) V_{sw} remained constant ($dV_{\text{sw}}/dt = 0$ within 5%). For the *ACE*/EPAM/DE4 data set the number of events in each group is (1) 36, (2) 81, and (3) 47 (for four events no solar wind data were available). For the *Ulysses*/HI-SCALE/

DE4 data set the number of events in each group is (1) 4, (2) 13, and (3) 38.

Figure 17 shows the scatterplots of τ versus (a)–(c) V_{sw} , (d)–(f) γ , and (g)–(i) τ_{theor} for the *ACE*/EPAM/DE4 data set.

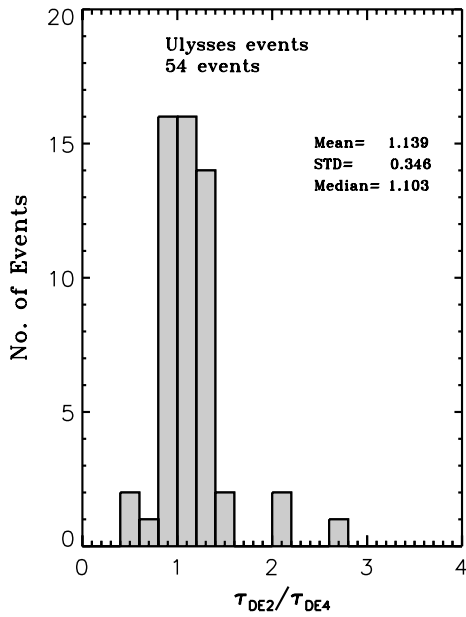


Figure 16. Distribution of the ratio between the decay rates from the data sets *Ulysses*/HI-SCALE/DE2 (τ_{DE2} ; Table 4) and *Ulysses*/HI-SCALE/DE4 (τ_{DE4} ; Table 3).

All of the $dV_{sw}/dt > 0$ cases show values of τ below 25 hr, whereas the $dV_{sw}/dt < 0$ and $dV_{sw}/dt = 0$ cases extend to larger τ values. The average value of τ for the $dV_{sw}/dt > 0$ cases is $\langle \tau \rangle = 11.0$ hr, whereas for the $dV_{sw}/dt < 0$ cases is $\langle \tau \rangle = 13.6$ hr, and for the $dV_{sw}/dt = 0$ cases is $\langle \tau \rangle = 19.8$ hr. Kecskeméty et al. (2009) also found a large scatter of τ values with respect to solar wind speed, V_{sw} (see their Figure 9). The average values of τ for low-energy protons were $\langle \tau \rangle = 16.5$ hr for those time intervals with monotonic increase of V_{sw} ($dV_{sw}/dt > 0$), significantly lower than for the cases with V_{sw} constant ($dV_{sw}/dt = 0$ within 5%) and V_{sw} decreasing ($dV_{sw}/dt < 0$) with $\langle \tau \rangle = 19.6$ hr and 19.1 hr, respectively (see their Figure 8).

The cases of increasing solar wind speed usually occur just after the passage of a low solar wind speed rarefaction region, whereas the decreasing or constant solar wind cases occur after the passage of a compression region. In terms of the scenario proposed by Sarris & Malandraki (2003) a compression region located beyond 1 AU may contribute to linger the decay phase of the near-relativistic electron events and hence the possibility of observing large values of τ for the $dV_{sw}/dt < 0$ cases. However, most of the events within each group of our data set have low τ values ($M_\tau = 9.45$ hr, $M_\tau = 11.16$ hr, $M_\tau = 15.22$ hr for the $dV_{sw}/dt > 0$, $dV_{sw}/dt < 0$, and $dV_{sw}/dt = 0$ cases, respectively). Sarris & Malandraki (2003) showed two cases of events with low and large τ for $dV_{sw}/dt > 0$ and $dV_{sw}/dt < 0$ cases respectively, that corresponded to the passage by 1 AU of a rarefaction region and a compression region before the onset of the event, respectively. A preliminary analysis of the solar wind structure observed before the onset of the event by 1 AU of the events for the *ACE*/EPAM/DE4 data set shows that this trend is not general and the study of Sarris & Malandraki (2003) was focused on two extreme cases. However, we would like to point out the limitations of single-point measurements to infer the existence of compression regions beyond the observer after their possible passage over the spacecraft. Uncertainties about (1) the evolution of these structures as they move away from the observer, (2) the magnetic connectivity between the spacecraft and these structures, and (3) the ability of these structures to

reflect particles back toward the observer remain obscured from the point of view of single-point measurements.

Figures 17(a)–(c) show that the few events with large values of τ ($\tau > 30$ hr) are not associated with high ($V_{sw} \gtrsim 550$ km s⁻¹) solar wind speeds, suggesting that either the decays in the high-speed solar wind streams are necessarily fast (i.e., low $\tau < 30$ hr) or that our data set does not contain a sufficient number of events observed in fast solar wind. The first option would indicate that convection with the solar wind (when this is fast) has an important effect in shaping the decay phase of the events (producing fast decays). The only possible dependence found by Kecskeméty et al. (2009) between τ and V_{sw} was that the highest values of τ do correlate with small values of V_{sw} whereas the highest values of V_{sw} correlate with small values of τ .

Figures 17(d)–(f) show the trend for γ to decrease with τ in the sense that long decay rates have small spectral index γ (i.e., a hard energy spectrum); or inversely particle intensities decay fast when the spectrum is soft, suggesting that adiabatic deceleration plays a role in shaping the decay phase of the event. Although not shown by Kecskeméty et al. (2009), these authors indicated that a similar dependence between τ and γ was found.

Finally, Figures 17(g)–(i) show the values of τ_{theor} versus τ . As pointed out by Forman (1970), for an observer at $R = 1$ AU the decay time τ_{theor} is fairly uniform from event to event since both V_{sw} and γ are not highly variable, and hence the cluster of points in Figures 17(g)–(i) around the same value of τ_{theor} . Contrary to Kecskeméty et al. (2009), who only used events with $dV_{sw}/dt \sim 0$ to compare τ with τ_{theor} , we do not find any correlation between τ and τ_{theor} (Figure 17(i)). According to Kecskeméty et al. (2008), the cases $\tau_{theor} < \tau$ at 1 AU with $dV_{sw}/dt \sim 0$ occur in events originated mostly from the eastern hemisphere as seen from the Earth, whereas the cases with $\tau_{theor} > \tau$ and $dV_{sw}/dt \sim 0$ are mostly associated with western events. Figure 17(i) shows that most of the events with $dV_{sw}/dt \sim 0$ (31 out of 47) had $\tau_{theor} > 1.3 \tau$ (i.e., they show as a point in the left upper edge of Figure 17(i) and outside of the area marked by the dashed lines that correspond to $\tau_{theor} = \tau$ with a margin of $\pm 30\%$). Of these 31 events we have identified the solar phenomena associated with the origin of 24 events and only three of them were originated eastward of E10. Figure 17(i) shows only five events in the lower right edge corresponding to cases with $\tau_{theor} < \tau$ and outside of the $\pm 30\%$ dashed lines. These five cases were the events 62 (W77), 74 (W12), 85 (W180; association made by Cliver et al. 2005), 110 (E90) and 158 (E100). Although the statistics are very meager, we find that most of the events with $dV_{sw}/dt \sim 0$ and generated from western longitudes tend to have $\tau_{theor} > \tau$; however, our data sample is biased because most of the events are generated from western longitudes (Figure 10) and show $\tau_{theor} > \tau$ (Figure 17(i)).

Since the expression of τ_{theor} deduced by Forman (1970) does not account for the variation of particle intensity due to the continuous transference of the observation point from flux tube to flux tube, Kecskeméty et al. (2009) interpreted the differences between τ_{theor} and τ in terms of the heliolongitude profile of the particle injection near the Sun. For eastern flares the observed decay rate is longer than that expressed by Equation (1) ($\tau_{theor} < \tau$) because the populated flux tubes of particles are convected over the spacecraft during the decay of the event. For western flares, the flux tubes populated by the centroid of the injection profile (assumed to be centered at the flare site) will not be observed by the spacecraft, and only the tail of this profile will be observed during the decay of the event, corresponding to

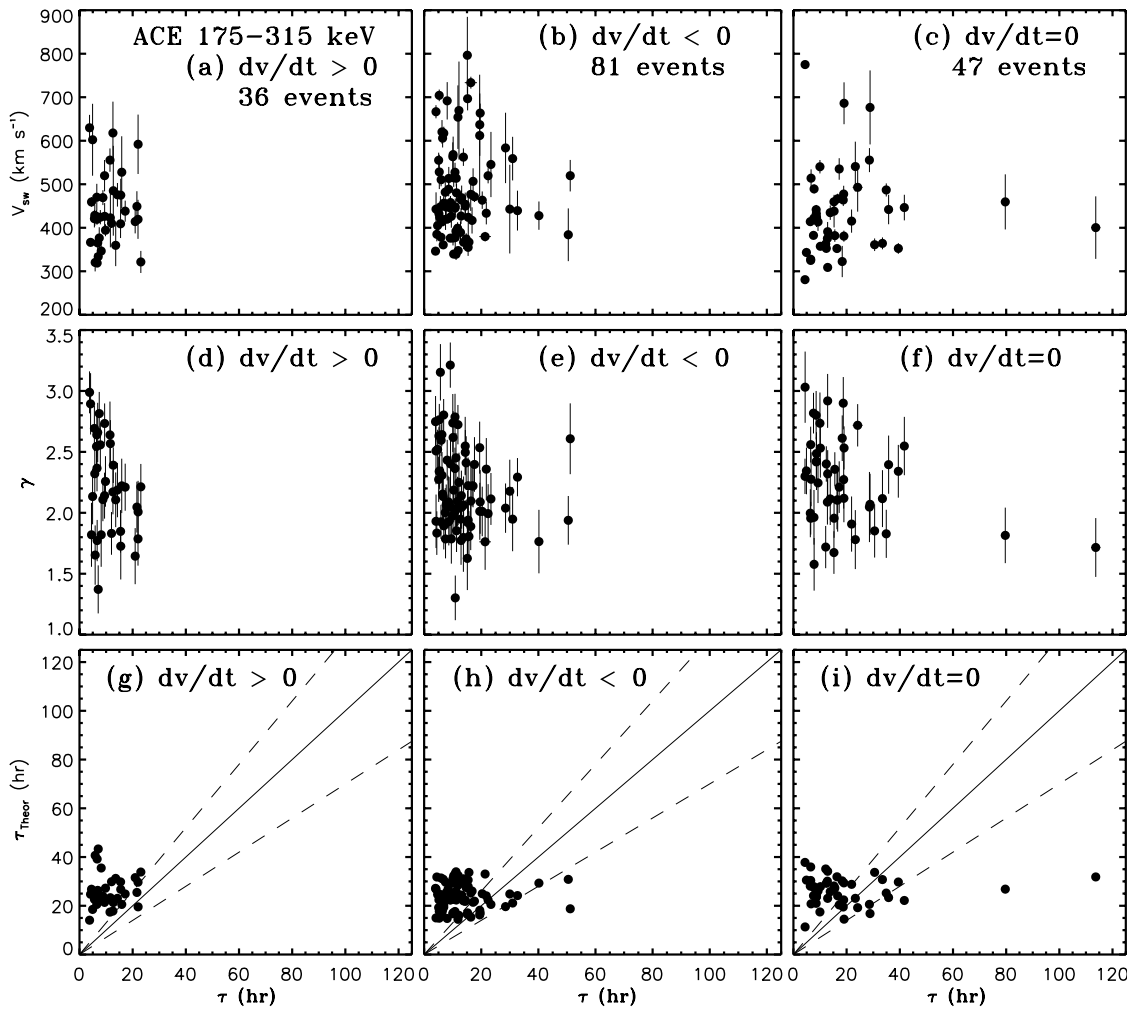


Figure 17. Correlations between τ and (a)–(c) V_{sw} , (d)–(f) γ , and (g)–(i) τ_{theor} for the *ACE/EPAM/DE4* data set distinguishing the events with increasing solar wind speed (left panels), decreasing solar wind speed (middle panels), and constant (within 5%) solar wind speed (right panels). The solid line in panels (g)–(i) indicates the case $\tau_{theor} = \tau$ and the dashed lines a 30% deviation with respect to the τ value.

decay rates τ shorter than τ_{theor} . Because of our selection criteria, most of the events in our data set are associated with western events (the distribution of heliolongitudes for those events with known origin (excluding the W+ events) has a mean value of $35^{\circ}8W$). The small number of eastern events with $dV_{sw}/dt \sim 0$, the lack of dependence between longitude and τ (Figure 10), and the general lack of agreement between τ_{theor} and τ does not allow us to confirm the longitude dependence suggested by Kecskeméty et al. (2008).

Figure 18 compares the values of τ with V_{sw} , γ , and τ_{theor} for the *Ulysses/Hi-SCALE/DE4* data set. Similarly to the *ACE* case (Figure 17), the few events with increasing V_{sw} (black solid symbols) are restricted to low decay rates ($\tau < 70$ hr), whereas the decreasing (open triangles) and constant (gray solid symbols) V_{sw} cases may extend to longer decay rates ($\tau > 100$ hr). Figure 18(a) shows that the long decay rates ($\tau > 100$ hr) are limited to low solar wind values ($V_{sw} < 500$ km s $^{-1}$) and no long decay rates are observed in fast solar wind streams. Similarly to the *ACE* case, Figure 18(b) shows that there is a trend for long decay rates to have hard energy spectra. Figure 18(c) compares the values of τ_{theor} with those of τ . Although the values of τ_{theor} are more spread than in the case of 1 AU (Figures 17(g)–(i)), there is no correlation between τ and τ_{theor} (only 10 decays show similar (within 30%) values of τ and τ_{theor} as indicated by the dashed lines in Figure 18(c)).

In summary, Figures 17 and 18 show that solar wind convection and adiabatic deceleration have a significant effect on the decay rate, but not as expressed by Equation (1) deduced by Forman (1970).

8. RADIAL, LONGITUDINAL, AND LATITUDINAL DEPENDENCE OF THE DECAY RATES

In order to study the radial dependence of decay rates in SEP events it is important to choose single SEP events that are concurrently observed by two spacecraft at two different radial distances. Most of the events observed by *Ulysses* result from a series of events seen at 1 AU that merge as a single event when observed at larger heliocentric distances (Lario et al. 2000). Therefore, it is difficult to find isolated events that allow us to compare the decay rates as observed at different radial distances (Lario 2010). Among the 55 events of the *Ulysses/Hi-SCALE/DE4* data set, we have selected (1) those events for which during its duration there is only a single electron increase at *ACE* (included in the *ACE/EPAM/DE4* data set) and presumably associated with the same solar origin as the event at *Ulysses* (i.e., the events 13^U , 14^U , 20^U , 26^U , 27^U , 28^U , 33^U , 39^U , 42^U of Table 3) and (2) those for which the onset of the event at *Ulysses* occurs in association with an event at *ACE* that is included in the *ACE/EPAM/DE4* data set (Table 1).

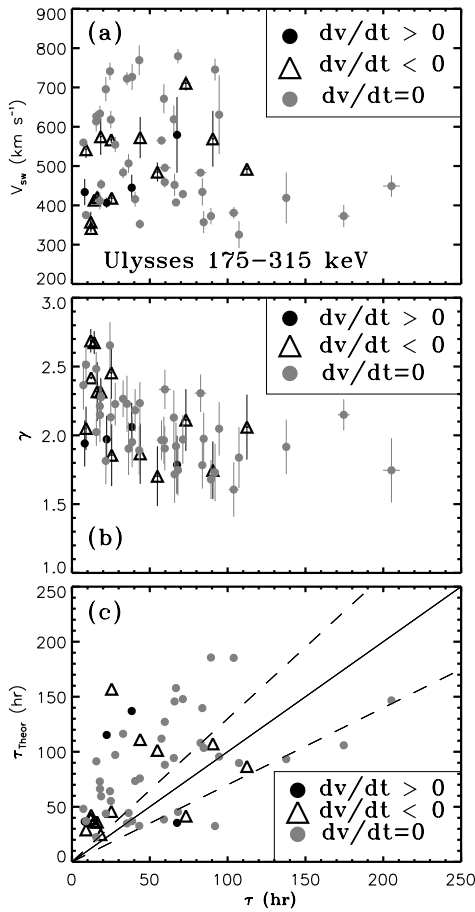


Figure 18. Same as Figure 17 for the *Ulysses*/HI-SCALE/DE4 data set.

and for which we assume that most of the events at *Ulysses* are produced by this main event at *ACE* (i.e., the events 2^U , 6^U , 10^U , 23^U , 30^U , 32^U , 35^U).

Table 6 lists the 16 events selected, together with the most likely solar flare associated with the origin of the SEP event at *ACE* and *Ulysses*. Column 1 lists the number of the events according to the *ACE*/EPAM/DE4 data set (Column 1 of Table 1). Column 2 lists the number of the events given in the *Ulysses*/HI-SCALE/DE4 data set (Column 1 of Table 3). Column 3 lists the solar flare most likely associated with the origin of the SEP event at *Ulysses* and *ACE*, first its H α location and the time of the onset of the 1–8 Å X-ray emission (in format year/day/hour:minute UT) as reported in the Solar Geophysical Data⁴. The table footnotes indicate when such association is made by other authors. Column 4 lists the *Ulysses*' heliocentric radial distance. Columns 5 and 6 give the heliographic latitude of *Ulysses* and Earth during these events, respectively (negative values indicate southern latitudes). Column 7 lists the range of longitudes (with respect to the Earth) spanned by *Ulysses* from the onset of the event to the end of the exponential decay (i.e., the end time of either $\Delta t_{\tau_{ACE}}$ or $\Delta t_{\tau_{Uly}}$, whichever is longer). Column 8 lists the cone angle between the nominal footpoints of the magnetic field lines intersecting *ACE* and *Ulysses* computed using daily averages of the measured solar wind at the two spacecraft as described by Hawkins et al. (2001). The range of values covers from the onset of the event until the end of the time interval Δt_{τ} (either $\Delta t_{\tau_{ACE}}$ or $\Delta t_{\tau_{Uly}}$, whichever is longer). Finally, Columns 9 and 10 provide the value of the decay rates

at *ACE* (τ_{ACE}) and *Ulysses* (τ_{Uly}) as listed in Columns 9 of Tables 1 and 3, respectively.

Most of the events in Table 6 (9 out of 16) occurred when *Ulysses* was at high latitudes ($|\Lambda_{Uly} - \Lambda_{Earth}| > 60^\circ$ either north or south). That implies that for most of the events the cone angle between the nominal footpoints of *ACE* and *Ulysses* ranges from $\sim 70^\circ$ to $\sim 120^\circ$. This large angular distance between the magnetic footpoints was not an impediment to observe common events at *ACE* and *Ulysses* suggesting that either broad sources of particles and/or an efficient cross-field diffusion of particles act as an efficient mechanism to distribute energetic particles throughout the heliosphere (Lario 2010).

Figure 19 shows the ratio of decay rates at *Ulysses* and *ACE* τ_{Uly}/τ_{ACE} as a function of (a) the *Ulysses*' heliocentric distance, (b) the latitudinal distance between the two spacecraft, (c) the longitudinal distance between the two spacecraft, and (d) the cone angle formed by the nominal footpoints of the two spacecraft. The black symbols are used for those events with single SEP injections at *ACE* and *Ulysses*. Figure 19(a) shows that, except for the event 91 (27^U), the events commonly observed by *Ulysses* at heliocentric radial distances $R < 2.6$ AU and by *ACE* at $R \sim 1$ AU have similar decay rates, i.e., $\tau_{Uly}/\tau_{ACE} < 1 \pm 0.3$. For those events observed in common when *Ulysses* was at distances $R < 3.0$ AU and *ACE* at $R \sim 1$ AU, we obtain $\tau_{Uly}/\tau_{ACE} < 1 \pm 0.45$ with the exception of the events 91 (27^U) and 56 (10^U). At larger heliocentric distances, Figure 19(a) clearly shows that $\tau_{Uly} > \tau_{ACE}$.

Keckskeméty et al. (2009) compared the decay rates of ~ 1 MeV and ~ 5 MeV proton events observed by *Ulysses* at low heliographic latitudes ($\Lambda \in [-10^\circ, +10^\circ]$) and at radial distances between 1.34 and 5.41 AU with the decay rate of those events observed simultaneously by *IMP-8* at 1 AU. Although a careful description of the selection of the events was not provided by Keckskeméty et al. (2009), these authors found a similar radial dependence as the one shown in Figure 19(a) (see their Figure 17). Keckskeméty et al. (2009) concluded that although a scatter of τ_{Uly}/τ_{ACE} values was found, an increase of τ with radial distance was observed between 2 and 5 AU.

Figure 19(b) shows that, with the exception of the events 91 (27^U) and 56 (10^U), the events commonly observed by *ACE* and *Ulysses* when the difference in heliographic latitude was larger than 57° (i.e., $|\Lambda_{Uly} - \Lambda_{ACE}| > 57^\circ$) show similar decay rates $\tau_{Uly}/\tau_{ACE} < 1 \pm 0.45$. This result should be interpreted in terms of the coincidental occurrence of intense large SEP events simultaneously observed by *ACE* close to the heliographic equator and by *Ulysses* during its high-latitude transits at the end of 2000 and 2001 (Lario et al. 2003; Lario 2010). Large isolated intense SEP injections occurred during these periods favoring the observation by *ACE* and *Ulysses* of common decay rates without the occurrence of new SEP injections (Lario 2010). The isolation of these events with respect to other intense SEP injections favored the observation of the reservoir effect (Lario 2010). Although reservoirs were observed also when *Ulysses* was at low latitudes and larger heliocentric distances (Lario 2010), the restrictive selection of events used here to study the decay of the events commonly observed by *ACE* and *Ulysses* results in the absence of low-latitude large-distance events with similar τ in Figure 19. As described in Section 1, the criteria used by Lario (2010) to determine when and where near-relativistic electron reservoirs were observed by *ACE* and *Ulysses* differ from the criteria used here to study the decay phase of the events. The criterion of similar intensities during reservoirs has not been checked in the present study. The reader is referred to

⁴ <http://www.swpc.noaa.gov>

Table 6
Ulysses and *ACE* Events in Common

(1)	(2)	(3)	(4)	(5)	(6)	(7)	(8)	(9)	(10)
# _{ACE}	# _{Uly}	Flare ^a	R_{Uly} ^b	Λ_{Uly}	Λ_{Earth}	Φ	Cone Ang.	τ_{ACE}	τ_{Uly}
6	2 ^U	S43W90 1998/110/09:31	5.41	-6°	-5°	294°-307°	128°-168°	22.00 ± 0.11	71.23 ± 0.44
24	6 ^U	N27E95 1999/020/19:06 ^c	5.17	-20°	-5°	35°-40°	91°-138°	34.90 ± 0.73	65.92 ± 1.17
56	10 ^U	S17W09 2000/256/11:31	2.78	-71°	7°	193°-198°	114°-115°	15.39 ± 0.42	40.59 ± 0.29
62	13 ^U	N10W77 2000/313/22:42	2.39	-79°	3°	180°-187°	90°-96°	113.69 ± 1.75	107.29 ± 0.99
68	14 ^U	S07E46 2001/020/21:06	1.88	-68°	-5°	188°-191°	63°-67°	32.68 ± 0.55	36.36 ± 0.60
82	20 ^U	S29W130 2001/166/15:20 ^c	1.37	25°	1°	74°-77°	82°-91°	23.07 ± 1.30	15.57 ± 0.54
85	23 ^U	S20W180 2001/227/23:35 ^d	1.65	64°	7°	29°-35°	102°-110°	79.67 ± 0.87	67.51 ± 0.37
90	26 ^U	N06W18 2001/308/16:03	2.20	77°	4°	63°-65°	83°-88°	50.46 ± 0.73	59.06 ± 0.42
91	27 ^U	S13E42 2001/321/04:49	2.28	75°	2°	61°-63°	86°-91°	12.86 ± 0.11	38.66 ± 0.80
92	28 ^U	S15W34 2001/326/22:32 ^c	2.33	73°	1°	55°-61°	81°-87°	29.98 ± 0.29	35.34 ± 0.21
94	30 ^U	N08W54 2001/360/04:32	2.56	66°	-2°	38°-39°	78°-80°	33.47 ± 1.02	25.28 ± 0.92
96	32 ^U	N13W02 2002/009/17:42 ^e	2.64	64°	-4°	24°-28°	75°-80°	51.15 ± 0.87	73.19 ± 2.91
97	33 ^U	N10W120 2002/027/12:30 ^f	2.76	61°	-6°	8°-12°	77°-98°	12.77 ± 0.60	17.89 ± 0.40
103	35 ^U	S14W84 2002/111/00:43	3.28	48°	-5°	279°-295°	51°-72°	40.18 ± 0.62	137.67 ± 0.85
113	39 ^U	N09E28 2002/248/16:18	4.00	33°	7°	162°-165°	31°-34°	18.89 ± 0.67	22.30 ± 0.77
129	42 ^U	S08E61 2003/168/22:27 ^c	4.97	13°	1°	241°-246°	62°-103°	9.96 ± 0.17	27.80 ± 0.34

Notes.

^a Solar flare most likely related to the origin of the SEP event at *ACE* and *Ulysses*. H α location and time of the onset of the 1–8 Å X-ray emission (in format year/day/hour:minute) as reported in Solar Geophysical Data.

^b Heliocentric radial distance of *Ulysses* in units of AU.

^c Flare association made by Cane et al. (2006).

^d Based on the association made by Cliver et al. (2005).

^e Cane et al. (2006) associated the origin of the event 96 with a C9 flare at E100 on 2002/008/18:14 UT.

^f Based on the occurrence of a halo CME as reported on http://cdaw.gsfc.nasa.gov/CME_list/.

Lario (2010) for details on the observation of reservoirs during the events shown in Figure 19.

Finally, Figures 19(c) and (d) show that there is no dependence between the decay rates at the two spacecraft and either the longitudinal distance between the two spacecraft or the cone angle sustained by the nominal magnetic footpoints of the two spacecraft, suggesting that at *Ulysses*' distances longitude is not an important factor to determine the common observation of decays at *Ulysses* and *ACE*.

9. CONCLUSIONS

The statistical analysis of the decay rates observed in solar near-relativistic electron events by *ACE* and *Ulysses* throughout solar cycle 23 leads us to the following results:

1. Events at 1 AU that have an associated intensity increase at *Ulysses* show on average larger decay rates (Figure 3), longer decays (Figure 6), larger peak intensities, and higher event fluences (Figures 4 and 7) than those events without an associated intensity increase at *Ulysses*. This result indicates that either only large intense events are observed simultaneously by *ACE* and *Ulysses* or that the events with shorter decays, small peak intensities, and faster decay rates do not last long enough to either be observed by *Ulysses* at large heliocentric distances or meet our selection criteria to be included in Table 3.
2. A correlation is found between the peak intensities and the fluence of the events at both *ACE* and *Ulysses* (Figures 4 and 12).
3. The events observed at *Ulysses* have, in general, longer decay rates (Figure 11) and longer decays (Figure 14) than those observed at *ACE*, but do not show any correlation between τ and either J_{peak} or F (Figure 13). Either long-decay events are required to be observed by *Ulysses* at larger heliocentric distances or the more numerous diffusion

processes undergone by the particles traveling to larger distances make the decay of the events longer.

4. Within our energy range (53–315 keV) we observe either an energy independence of the decay rate or slightly longer decays at lower energies at both *ACE* and *Ulysses* (Figures 8 and 16). These results indicate an invariant spectrum during the decay of most of the near-relativistic electron events (at least in our energy range). If electrons observed during the decay phase are confined in an expanding volume, the faster the electrons the more likely to escape from the expanding volume and hence that τ decreases with electron energy. If decays are dominated by adiabatic deceleration, the steeper the spectrum the faster the decay of intensities.
5. Whereas the longitude of the associated parent solar event influences the observation of either one or two phases in the decay of the events at 1 AU, there is no general dependence between the decay rate τ and the longitude of the parent solar event (Figure 10). The exception is for nominal well-connected longitudes where events with faster decay rates are more common than for the rest of poorly-connected longitudes. Events with narrow particle injections (i.e., fast decays) require a good connection between the spacecraft and the particle sources in order to be observed. Well-connected events are more likely to show two phases in their decay, the first phase characterized by a fast decay rate is most likely to result from strong longitudinal gradients of the particle injection near the flare site. For poorly-connected events the decay rates are generally longer since the spatial gradients of the particle injection have been smoothed out by more extended sources.
6. Within our statistics, we observe an absence of long decay rates in fast solar wind streams (Figures 17 and 18) suggesting that solar wind convection plays a role in shaping the decay of the events (fast solar wind implies a fast decay in particle intensities).

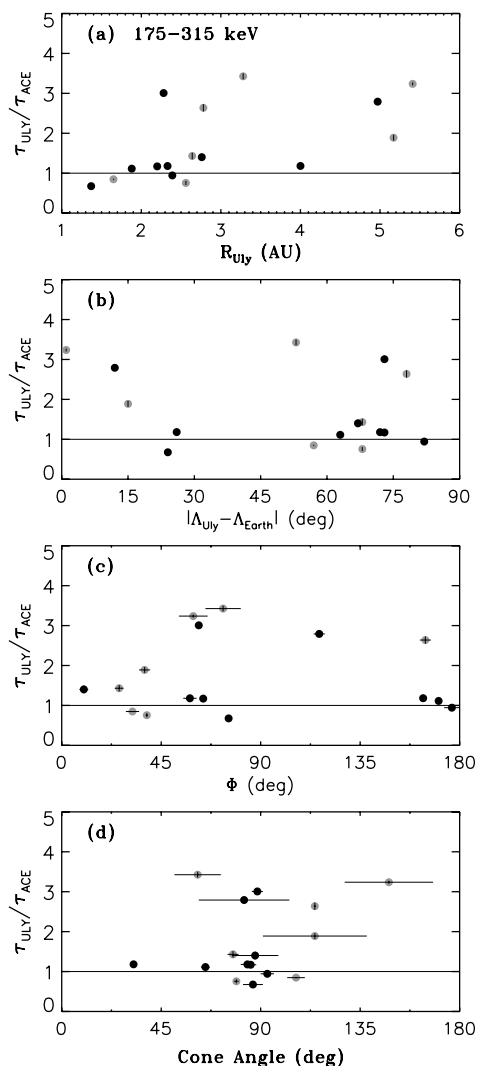


Figure 19. Ratio of the decay rates at *Ulysses* and *ACE* for the events listed in Table 6 as a function of the (a) *Ulysses*' heliocentric radial distance, (b) latitudinal angular distance between *ACE* and *Ulysses*, (c) *Ulysses*' longitude with respect to the Earth, and (d) cone angle between the *Ulysses* and *ACE* nominal magnetic footpoints. The black symbols are used for those events with single injections at *ACE* and *Ulysses*, whereas the gray symbols are used for those events showing multiple injections at *ACE*. See the text for details.

7. There is a trend to observe small spectral index γ (i.e., a hard spectrum) for events with long decay rates suggesting that adiabatic cooling plays a significant role during the decay phase of SEP events (Figures 17 and 18).
8. The expression deduced by Forman (1970) assuming only the effects of solar wind convection and adiabatic deceleration over an isotropic distribution with small spatial gradients is not directly applicable for comparison with the observed decay rates (Figures 17 and 18). Therefore, more processes than those considered by Forman (1970) may be acting during the decay phase of solar near-relativistic electron events.
9. Using a restrictive criterion to select those events commonly observed by *ACE* and *Ulysses*, we observe that, with the exception of two events, the events observed when *Ulysses* was at distances $R < 3.0$ AU show similar decay rates at *ACE* and *Ulysses*, implying, in the case that the intensities at the two spacecraft were similar, the observation of energetic particle reservoirs (Lario 2010). Those events occurred mainly when *Ulysses* was at high

heliolatitudes ($|\Lambda| > 57^\circ$ with respect to the Earth), whereas the events at lower latitudes showed complex-time-intensity profiles and different decay rates were observed at *ACE* and *Ulysses*. The coincidental occurrence of large isolated SEP events when *Ulysses* was at high heliolatitudes favored the observation of heliospheric energetic particle reservoirs. For distances $R > 3$ AU the decay rates were always longer at *Ulysses* than at *ACE* suggesting that diffusion processes undergone by particles as they move to longer distances contribute to linger the decay of the events.

The author acknowledges the support from NSF under SHINE research grant ATM-0648181 and NASA under HGI grant NNX09AG30G. Thanks are due to Jennifer A. Thorne (Summer Intern at JHU/APL) for her help.

REFERENCES

- Agueda, N., Vainio, R., Lario, D., & Sanahuja, B. 2008, *ApJ*, **675**, 1601
- Anderson, K. A., & Lin, R. P. 1966, *Phys. Rev. Lett.*, **16**, 1121
- Anderson, K. A., Sommers, J., & Lin, R. P. 1995, *J. Geophys. Res.*, **100**, 3
- Bame, S. J., et al. 1992, *A&AS*, **92**, 237
- Burlaga, L. F. 1967, *J. Geophys. Res.*, **72**, 4449
- Cane, H. V., Mewaldt, R. A., Cohen, C. M. S., & von Rosenvinge, T. T. 2006, *J. Geophys. Res.*, **111**, A06S90
- Cliver, E. W., et al. 2005, *Proc. 29th ICRC*, **1**, 121
- Daibog, E. I., et al. 2003, *Adv. Space Res.*, **32**, 2655
- Daibog, E. I., et al. 2009, *Bull. Russ. Acad. Sci.*, **73**, 319
- Dröge, W. 2000, *Space Sci. Rev.*, **93**, 121
- Englade, R. C. 1971, *J. Geophys. Res.*, **76**, 768
- Forman, M. A. 1970, *J. Geophys. Res.*, **75**, 3147
- Forman, M. A. 1971, *J. Geophys. Res.*, **76**, 759
- Gold, R. E., et al. 1998, *Space Sci. Rev.*, **86**, 541
- Hawkins, S. E., Roelof, E. C., Decker, R. B., Ho, G. C., & Lario, D. 2001, *Space Sci. Rev.*, **97**, 269
- Krimigis, S. M. 1965, *J. Geophys. Res.*, **70**, 2943
- Keckskeméty, K., Daibog, E. I., Logachev, Y. I., & Kóta, J. 2008, *Proc. 30th ICRC*, **1**, 139
- Keckskeméty, K., Daibog, E. I., Logachev, Y. I., & Kóta, J. 2009, *J. Geophys. Res.*, **114**, A06102
- Lanzerotti, L. J., et al. 1992, *A&AS*, **92**, 349
- Lario, D. 2007, in *Highlights of Spanish Astrophysics IV, Proc. 7th Scientific Meeting of the Spanish Astronomical Society*, ed. F. Figueras et al. (Dordrecht: Springer), 295
- Lario, D. 2010, in *AIP Conf. Proc. 1216, 12th Int. Solar Wind Conf.*, ed. M. Maksimovic et al. (Melville, NY: AIP), 625
- Lario, D., et al. 2000, *J. Geophys. Res.*, **105**, 18251
- Lario, D., Roelof, E. C., Decker, R. B., & Reisenfeld, D. B. 2003, *Adv. Space Res.*, **32**, 579
- Lee, M. A. 2000, in *AIP Conf. Proc. 528, Acceleration and Transport of Energetic Particles Observed in the Heliosphere, ACE-2000 Symposium*, ed. R. A. Mewaldt et al. (Melville, NY: AIP), 3
- Lupton, J. E., & Stone, E. C. 1973, *J. Geophys. Res.*, **78**, 1007
- McComas, D. J. 1998, *Space Sci. Rev.*, **86**, 563
- McCracken, K. G. 1971, *Solar Phys.*, **18**, 100
- McKibben, R. B. 1972, *J. Geophys. Res.*, **77**, 3957
- McKibben, R. B., et al. 2003, *Ann. Geophys.*, **21**, 1217
- Meyer, P., Parker, E. N., & Simpson, J. A. 1956, *Phys. Rev. Lett.*, **104**, 768
- Owens, A. J. 1979, *J. Geophys. Res.*, **84**, 4451
- Reinhard, R., Roelof, E. C., & Gold, R. E. 1986, in *The Sun and the Heliosphere in Three Dimensions*, ed. R. G. Marsden (Dordrecht: Reidel), 297
- Roelof, E. C. 1969, in *Lectures in High-Energy Astrophysics*, ed. H. Ögelman & J. R. Wayland (NASA SP-199; Washington, DC: NASA), 111
- Roelof, E. C. 1975, *Proc. 14th ICRC*, **5**, 1716
- Roelof, E. C., et al. 1992, *Geophys. Res. Lett.*, **19**, 1243
- Ruffolo, D. 1995, *ApJ*, **442**, 861
- Sarris, E. T., & Malandraki, O. E. 2003, *Geophys. Res. Lett.*, **30**, 2079
- Simnett, G. M. 2001, *Space Sci. Rev.*, **97**, 231
- Simnett, G. M., Roelof, E. C., & Haggerty, D. K. 2002, *ApJ*, **579**, 854
- van Allen, J. A., & Krimigis, S. M. 1965, *J. Geophys. Res.*, **70**, 5737
- Yashiro, S. 2004, *J. Geophys. Res.*, **109**, A07105